Biogeosciences Discuss., doi:10.5194/bg-2016-399, 2016
Manuscript under review for journal Biogeosciences
Published: 4 October 2016

Biogeosciences Discussions
Open Access
EGU

Implications of sea-ice biogeochemistry for oceanic production and emissions of dimethylsulfide in the Arctic

Hakase Hayashida[1], Nadja Steiner[2], Adam Monahan[1], Virginie Galindo[3], Martine Lizotte[4], and Maurice Levasseur[4]

[1]School of Earth and Ocean Sciences, University of Victoria, Victoria, British Columbia, Canada
[2]Institute of Ocean Sciences, Fisheries and Oceans Canada, Sidney, British Columbia, Canada
[3]Centre for Earth Observation Science, Faculty of Environment, Earth and Resources, University of Manitoba, Winnipeg, Manitoba, Canada
[4]Département de biologie, Québec-Océan, Université Laval, Québec, Québec, Canada

Correspondence to: Hakase Hayashida (hakase@uvic.ca)

Abstract. Sea ice represents an additional oceanic source of the climatically active gas dimethylsulfide (DMS) for the Arctic atmosphere. To what extent this source contributes to the dynamics of summertime Arctic clouds is however not known due to scarcity of field measurements. In this study, we developed a coupled sea ice-ocean ecosystem-sulfur cycle model to investigate the potential impact of bottom-ice DMS and its precursor dimethylsulfoniopropionate (DMSP) on the oceanic production and emission of DMS in the Arctic. The result of the 1-D model simulation was compared with field data collected during May and June of 2010 in Resolute Passage. Our result reproduced the accumulation of DMS and DMSP in the bottom ice during the development of an ice algal bloom. The flushing of these sulfur species took place predominantly during the earlier phase of the melt period, resulting in an increase of DMS and DMSP in the underlying water column prior to the onset of an under-ice phytoplankton bloom. Processes that dominated the budgets of bottom- and under-ice DMS and DMSP were identified through an analysis of production and removal rates of processes considered in the model. When openings in the ice were taken into account, the simulated sea-air DMS flux during the melt period was dominated by episodic spikes of up to 5.6 μmol m^{-2} d^{-1}. Further model simulations were conducted to assess the effects of the incorporation of sea-ice biogeochemistry on DMS production and emissions, as well as the sensitivity of our results to changes of uncertain model parameters of the sea-ice sulfur cycle. The results highlight the importance of taking into account both the sea-ice sulfur cycle and ecosystem in the flux estimates of oceanic DMS near the ice margins and identify key uncertainties in processes and rates that would be better constrained by new observations.

1 Introduction

Dimethylsulfide (DMS) is a volatile biogenic trace gas that is produced primarily through ecological interactions encompassing marine planktonic and microbial food webs (Simo, 2001). Oceanic emissions of DMS are the largest natural source of sulfur in the atmosphere (Bates et al., 2004), thereby playing a crucial role in global sulfur cycling. Oceanic DMS emissions also play an important role in climate because oxidation products of DMS can serve as atmospheric aerosols and cloud condensation nuclei

Biogeosciences Discuss., doi:10.5194/bg-2016-399, 2016
Manuscript under review for journal Biogeosciences
Published: 4 October 2016

(CCN), therefore contributing to radiative forcing (Shaw, 1983). In 1987, Charlson et al. hypothesized that enhanced oceanic DMS emissions due to global warming could produce a negative feedback via increased scattering of incoming shortwave radiation by DMS-derived aerosols and CCN. Although this climate regulation by oceanic DMS emissions has been suggested to be unlikely on a global scale (Quinn and Bates, 2011), oceanic DMS emissions could still exert a significant influence on local climate in certain regions, such as the Arctic (Chang et al., 2011; Levasseur, 2013).

During the mid-spring and summer (May-August), the Arctic atmosphere becomes relatively free of anthropogenic aerosols due to increased wet deposition and decreased transport from lower latitudes, while concentrations of methanesulfonic acid (MSA), an oxidation product of DMS, increase and peak at various locations north of 70° N (Sharma et al., 2012). The cleansing of the summertime Arctic atmosphere promotes new particle formation and the presence of relatively high concentrations of MSA points towards oceanic DMS as the driver for the formation of summertime Arctic clouds (Leaitch et al., 2013). Simultaneous measurements of sea surface and atmospheric DMS concentrations provide further evidence linking new particle formation events to oceanic DMS emissions (Chang et al., 2011; Rempillo et al., 2011).

In addition to DMS produced within the water column, the presence of sea ice provides an additional source of oceanic DMS in the Arctic that can make a transient but potentially important contribution to the formation of sulfur-containing aerosols and clouds during the melt period (Levasseur et al., 1994; Levasseur, 2013; Mungall et al., 2016). Especially during spring (April-June), DMS and its precursor dimethylsulfoniopropionate (DMSP) can reach very high concentrations at the bottom layer of Arctic sea ice throughout the development of the ice algal bloom (Levasseur et al., 1994). Measurements of DMS and DMSP reveal concentrations in the bottom ice that are often 1 to 3 orders of magnitude larger than in the under-ice and open water columns (Kirst et al., 1991; Levasseur et al., 1994; Uzuka, 2003; Levasseur, 2013; Galindo et al., 2014, 2015). How much of this ice-related DMS eventually reaches the atmosphere is not known, but mechanisms have been suggested by which the DMS produced in the bottom ice supplies pulses of DMS into the pristine Arctic atmosphere during spring and therefore contributes significantly to the formation of new clouds in the Arctic (Levasseur et al., 1994). However, it is difficult in practice to measure the sea-air flux of DMS originating from the bottom ice alone and therefore to quantify the contribution of that flux relative to DMS produced within the water column. Process models can aid the understanding of the relevance of specific processes to the Arctic marine sulfur cycle as well as their likely spatio-temporal variability. To the best of our knowledge, only one previous study has incorporated the sea-ice sulfur cycle in model simulations (Elliott et al., 2012).

We hypothesize that DMS and DMSP produced in the bottom ice can make a substantial contribution to the production and emission of oceanic DMS in the Arctic. To test this hypothesis, we developed a sulfur cycle module for the bottom ice and underlying water column. This module was embedded into a coupled sea ice-ocean ecosystem model to conduct various simulations which were compared to observations within landfast first-year ice in Resolute Passage during 2010. The rest of this study is structured as follows: Section 2 provides the model description and the set up of the simulations; Section 3 provides the results of the standard run validated by the field measurements, as well as the results of the sensitivity runs exploring various aspects of the simulations; and Section 4 presents the conclusions.

Biogeosciences Discuss., doi:10.5194/bg-2016-399, 2016
Manuscript under review for journal Biogeosciences
Published: 4 October 2016

2 Model description and experimental design

A sulfur cycle module for the bottom ice and the water column was developed and embedded into an existing coupled sea ice-ocean ecosystem model. The resulting coupled model was applied in a one-dimensional (1-D) configuration to conduct simulations of DMS and DMSP dynamics within and under the bottom layer of landfast first-year ice in Resolute Passage during 2010.

2.1 Ecosystem model

The coupled sea ice-ocean ecosystem model is described and evaluated in Mortenson et al. (Submitted). In this earlier study, the model was used to study the physical and biological controls on the ice algal and under-ice phytoplankton blooms observed in Resolute Passage during the spring of 2010. The sea-ice component of the model consists of four prognostic variables including nitrate, ammonium, silicate, and ice algae. The model simulates the growth and decline of ice algae in the bottom layer of the sea ice, as well as the release of ice algae into the water column during the melt period. The oceanic component of the model is a ten-compartment (nitrate, ammonium, silicate, small and large phytoplankton, small and large zooplankton, small and large detritus, and particulate silica) lower-trophic level ecosystem model derived from Steiner et al. (2006). In the uppermost layer of the water column, the ocean ecosystem model is coupled to the sea-ice ecosystem model to represent the diffusive exchange of nutrients at the ice-water interface, as well as the release of living and dead ice algae into the water column as large phytoplankton and large detritus, respectively. The ecosystem dynamics are driven by physical processes which are computed by a coupled sea ice-ocean physical model. The oceanic component of this model is the General Ocean Turbulence Model (GOTM), a public domain 1-D water column model (Burchard et al., 1999, 2006). The sea-ice component is based on the 1-D thermodynamic model developed by Flato and Brown (1996), which is implemented into the GOTM framework with a modified parameterization of radiative transfer through sea ice (Abraham et al., 2015).

2.2 Sulfur cycle module

The structural design of the coupled sea ice-ocean sulfur cycle module developed in this study was inspired mainly by two previous marine sulfur cycle models (Archer et al., 2004; Steiner and Denman, 2008). It should be emphasized that sulfur cycle represented in this study (as well as in the models of the earlier studies) considers the cycling between DMSP and DMS only. Figure 1 shows the variables and processes represented in the module that are deemed most relevant for the production and removal of DMSP and DMS in the bottom ice and water column. DMSP in particulate (DMSPp) and dissolved (DMSPd) phases are simulated separately as they have distinct physical properties and ecological roles in sulfur cycling. For example, DMSPp released from the bottom ice is expected to sink quickly through the water column, whereas DMSPd likely remains in the under-ice meltwater lens upon its release from the bottom ice (Galindo et al., 2014, 2015). Furthermore, only DMSPd can be assimilated by bacteria to produce DMS (Stefels et al., 2007). In the model, DMSPp is simulated diagnostically by assuming a fixed intracellular DMSP:Chlorophyll a (Chl a) ratio for each of the simulated algal groups, while DMSPd and DMS are simulated prognostically. DMSPd is produced by cell lysis and exudation, and in the case of the water column, by

Biogeosciences Discuss., doi:10.5194/bg-2016-399, 2016
Manuscript under review for journal Biogeosciences
Published: 4 October 2016

sloppy feeding, while it is removed by bacterial consumption and free DMSP-lyase. DMS is produced by bacterial conversion and free DMSP-lyase, while it is removed by bacterial consumption, photolysis, and in the case of an ice-free water column, by sea-to-air flux. Additionally, in the water column, all sulfur species are mixed between model layers with eddy diffusivities computed by the ocean physical model. The sulfur species in the bottom ice and underlying water column are coupled one way through the flushing of DMSP-containing ice algae, DMSPd, and DMS in the bottom ice due to melting of snow and ice, which respectively produce fluxes to DMSP-containing large phytoplankton, DMSPd, and DMS in the uppermost layer of the water column. The concentrations of simulated sulfur species are computed at each model layer by a system of differential equations representing the budgets of these species, with parameterized expressions for the processes discussed above. A detailed description of the sulfur cycle module is presented in Appendix A.

It is worth noting the processes that may potentially be important to the sulfur cycle but are neglected in the present study. The release of simulated bottom-ice sulfur species into the water column due to gravitational drainage of brine is not accounted in the flushing term, as it requires a relatively complex parameterization (Vancoppenolle et al., 2010). Although the previous model study of the sea-ice sulfur cycle considered the production of DMSPd by sloppy feeding as an important DMSPd production term in the bottom ice (Elliott et al., 2012), this process is neglected in the present study as zooplankton grazing on ice algae is ignored (Mortenson et al., Submitted). The production of DMS by dimethylsulfoxide (DMSO) reduction in the bottom ice and water column is unconsidered due to the lack of observational constraints on this process, although it has been suggested to be a major pathway for DMS production in Antarctic sea ice (Asher et al., 2011). A possible direct release of DMS by intra- or extra-cellular DMSP-lyase activity of algae (Niki et al., 2000; Stefels, 2000; Alcolombri et al., 2015) is also disregarded. To the best of our knowledge, no studies as of yet have shown that diatoms, the dominant group of the bottom-ice algal community, possess or use DMSP-lyases. Finally, due to the lack of observational constraints, the emissions of DMS from snow, ice, and melt ponds are not taken into account in the DMS flux calculation, although previous studies suggest a potential importance of these fluxes (Zemmelink et al., 2008; Nomura et al., 2012; Levasseur, 2013; Mungall et al., 2016).

2.3 Model setup

Model simulations were conducted for the Arctic Ice-Covered-Ecosystem field campaign (Arctic-ICE), which took place between May and June of 2010 in Resolute Passage (74°42.6' N and 95°15' W; see Galindo et al., 2014 and Mundy et al., 2014). Data from this campaign were used to calibrate the parameters of the sulfur cycle model. The vertical domain of the model was divided into 10 uniformly spaced layers for the sea ice and 100 uniformly spaced layers for the upper 100 m of the water column. The model was integrated with a time step of 10 minutes from 1 February to 6 July, 2010. At the surface, the model was forced with Environment Canada's hourly weather data (including surface air temperature, zonal and meridional wind at 10 m above the sea surface, surface air pressure, relative humidity, cloud cover, and precipitation; http://climate.weather.gc.ca/) collected at Resolute airport, which is located within 7 km of the study site. Simulated temperature, salinity, and horizontal velocity fields were restored over the entire water column to the output of a 3-D regional model simulation (NEMO-LIM2; Dukhovskoy et al., 2016) with restoring timescales of 1 day for temperature and salinity, and 10 minutes for horizontal velocity fields. The initial snow and melt pond depths and ice thickness were set to 5, 0, and 55 cm, respectively. The thickness

Biogeosciences Discuss., doi:10.5194/bg-2016-399, 2016
Manuscript under review for journal Biogeosciences
Published: 4 October 2016

of the bottom-ice skeletal layer (in which the ecosystem and sulfur processes take place) was set to 3 cm to match with observations (Galindo et al., 2014). The initial biomass of ice algae was set to 3.5 μg Chl a L^{-1}. The initial concentrations of nitrate and silicate in the bottom ice and water column were respectively set to 7.2 μmol N L^{-1} and 14.7 μmol Si L^{-1}, based on measurements at the beginning of the Arctic-ICE 2010 field campaign (Mundy et al., 2014). The initial concentrations of ammonium in the bottom ice and water column, as well as the remaining ocean ecosystem model variables were set to 0.01 μmol N L^{-1} (μmol Si L^{-1} for particulate silica). The initial concentrations of DMSPd and DMS were assumed to be small, and were set to 0.1 nmol S L^{-1} in the bottom ice and water column.

2.4 Model experiments

Two types of model simulations were conducted in this study: standard and sensitivity runs. The standard run was designed to simulate the observed variability of physical and biogeochemical variables during the Arctic-ICE 2010 field campaign. Specifically, the performance of the standard run was evaluated by directly comparing the simulated results with the observed time series of snow and melt pond depths, ice thickness, Chl a, DMSPp and DMSPd in the bottom ice and upper water column. The default values of the sulfur cycle model parameters (Table 1) were calibrated to match the observations, starting from initial guesses based on available field measurements in Arctic waters.

Three types of sensitivity runs were designed to assess the impact of sea-ice biogeochemistry on the production and emission of DMS under the ice. The first experiment evaluated the changes in the simulated under-ice DMSPd and DMS concentrations due to the incorporation of sea-ice biogeochemistry. The second experiment explored the model uncertainty resulting from uncertainties in the parameters of the sea-ice sulfur cycle. The third experiment quantified the potential sea-air fluxes of DMS through openings in the ice during the melt period and the relative contributions of the sea-ice sulfur cycle and ecosystem to those fluxes. Details of the sensitivity runs are described in Section 3.2.

3 Results and discussions

3.1 Standard run

3.1.1 Snow and melt pond depths and sea ice thickness

Figure 2a shows the simulated and observed time series of snow and melt pond depths and ice thickness. It is important to note that our model accounts for subgrid-scale snow depth variability (Abraham et al., 2015), hence the simulated results are intended to represent the areal average over the study site. Because the observations were taken at multiple locations with different snow depths on most days, the mean of these observations can be directly compared with the simulated results. During the winter and spring, the simulated snow depth increased as a result of occasional snowfall events until it reached about 20 cm in mid-May (black solid line; Fig. 2a). This maximum depth is close to the observed site-average snow depth (black dots; Fig. 2a). Simulated snow started melting at the end of May, and had disappeared completely by mid-June. The simulated snow depth is within the observed range (black vertical bars; Fig. 2a). The resulting melt water from the simulated snow contributed

Biogeosciences Discuss., doi:10.5194/bg-2016-399, 2016
Manuscript under review for journal Biogeosciences
Published: 4 October 2016

to the formation of simulated melt ponds that reached a mean depth of about 4 cm in late June (black dashed line; Fig. 2a). The timing of simulated melt pond formation is reasonable as melt ponds with similar depths were observed during the last two days of sampling, as indicated by the negative values in the observed snow depth range. The simulated ice thickness increased gradually until it reached about 145 cm in early June (red line; Fig. 2a). Simulated ice melt started shortly after the initiation of snowmelt and was complete by early July. The observed range of ice thickness was small indicating its homogeneity over the study site (red vertical bars; Fig. 2a), and is comparable to the simulated values. Furthermore, the timing of the simulated ice disappearance is close to the timing of the ice breakup observed in the field (mid-July; Galindo et al., 2014). However, it should be noted that the ice thickness variation is driven solely by thermodynamic processes in the model, while mechanical processes (e.g. advection, ridging, and rafting) were likely also important at the study site.

3.1.2 Ice algal and phytoplankton biomass

Figure 2b shows the simulated and observed time series of ice algal biomass in the bottom 3 cm of the sea ice and phytoplankton biomass averaged over the upper 10 m of the water column. The simulated ice algal biomass increased gradually from late March and reached about 1050 μg Chl a L^{-1} by mid-May (black line; Fig. 2b). The simulated ice algal biomass did not increase further during the remainder of May due to nitrogen limitation and decreased rapidly due to flushing during the melt period in June (Mortenson et al., Submitted). The simulated ice algal bloom terminated in late June, about two weeks prior to the simulated ice breakup (red line; Fig. 2a). Both the magnitude and temporal variations in the simulated ice algal bloom are generally comparable with the observations at the study site (black dots; Fig. 2a).

In the upper 10 m of the water column, the simulated phytoplankton biomass started increasing in early June and quickly reached a peak of about 10.5 μg Chl a L^{-1} in mid-June (red line; Fig. 2b). This simulated under-ice phytoplankton bloom was dominated by large cells and terminated due to nitrogen limitation (Mortenson et al., Submitted). These findings are consistent with the observations that reported that the bloom was numerically dominated by centric diatoms and led to the complete use of nitrate and nitrite (down to about 0.1 μmol L^{-1}) in the upper 10 m of the water column (Mundy et al., 2014). The timing and magnitude of the simulated under-ice phytoplankton bloom are comparable with the observations (red dots; Fig. 2b).

3.1.3 DMSPp, DMSPd, and DMS concentrations

Figure 3a shows the simulated and observed time series of the bottom-ice (3 cm) DMSPp concentration and the seawater DMSPp concentration averaged over the upper 10 m of the water column. The simulated DMSPp concentrations were determined by assuming fixed DMSPp-to-Chl a ratios (Eq. (A1) and Eq. (A13)), as the observations in Resolute Passage showed a strong linear relationship betwen DMSPp and Chl a concentrations both in the bottom ice and in the underlying water column (Galindo et al., 2014). Therefore, the temporal variability in simulated DMSPp was identical to that of simulated ice algal and phytoplankton biomass (black and red lines; Fig. 2b), respectively. The simulated bottom-ice DMSPp concentration reached about 10^4 nmol L^{-1} at the peak of the simulated ice algal bloom in mid-May (black line; Fig. 3a). The observed bottom-ice DMSPp concentrations were highly variable during this period both spatially (vertical bars associated with black dots on each sampling day; Fig. 3a) and temporally (the range of black dots; Fig. 3a). The simulated bottom-ice DMSPp

Biogeosciences Discuss., doi:10.5194/bg-2016-399, 2016
Manuscript under review for journal Biogeosciences
Published: 4 October 2016

concentrations were close to the site-average value observed on day 2, near the lower end of the observed range on day 3, and close to the upper ends of the observed range on days 4, 6, and 7 of the sampling during May (black dots and associated vertical lines; Fig. 3a). During the melt period in June, the temporal variations in simulated bottom-ice DMSPp concentration closely followed the observed site-average values sampled on the last four days (black dots; Fig. 3a). In the upper 10 m of the water column, the simulated seawater DMSPp concentration started increasing in June and peaked at about 100 nmol L^{-1} in mid-June (red line; Fig. 3a), coinciding with the simulated under-ice phytoplankton bloom (red line; Fig. 2b). The simulated values were close to the observed values throughout the sampling period except for days 2 and 3 (red dots; Fig. 3a); on the second and third sampling days in early May, the observed site-average DMSPp concentrations in the upper 10 m of the water column were about 20 nmol L^{-1}, while the simulated DMSPp was nearly 0 nmol L^{-1}. Galindo et al. (2014) attributed this abrupt DMSPp increase to the release of ice algae from the bottom ice. Although the model simulated the release of ice algae during the same time period, it did not result in a significant enhancement of simulated DMSPp in the water column because in the model the majority of the flushed ice algae enter the large detritus pool which was assumed to possess no intracellular DMSP. The model's inability to simulate this feature, however, conceivably had negligible impacts on the simulated sulfur cycle dynamics in the near-surface water column as the sloughed DMSP-containing ice algae are likely to sink through the water column fairly quickly. This argument is supported by a rapid decrease (to nearly 0 nmol L^{-1}) in the observed DMSPp in the upper 10 m of the water column on the following sampling day (i.e. day 4).

Figure 3b shows the simulated and observed time series of the bottom-ice DMSPd concentration and the seawater DMSPd concentration averaged over the upper 10 m of the water column. The simulated bottom-ice DMSPd concentrations gradually increased from early April to late May with a peak of about 1800 nmol L^{-1} (black line; Fig. 3b). During the melt period, the simulated bottom-ice DMSPd concentration decreased gradually and reached nearly 0 nmol L^{-1} by late June. The simulated bottom-ice DMSPd closely followed the observed site-average values except for high values (ca. 5000 nmol L^{-1}) measured during the first three sampling days (black dots; Fig. 3b). Potential explanations of the model-data mismatch include: the observed value on day 1 does not represent the site average because the sampling was done only at a single site (as opposed to three sites of different snow cover) which also explains the standard deviation of zero; and the observed site-average value on day 2 was associated with extremely large spatial variability (0-10^4 nmol L^{-1}). The model was unable to reproduce the observed values on day 3, which were consistently high at all sites and for all bottom-ice variables (ice algal biomass, DMSPp, and DMSPd). In the upper 10 m of the water column, the simulated DMSPd concentrations were nearly 0 nmol L^{-1} until the onset of simulated under-ice bloom in June (red line; Fig. 2b). In contrast, the observed site-average DMSPd concentrations were above 1 nmol L^{-1} for four consecutive sampling days (from day 3 to 6) in May (red dots; Fig. 3b). This observed DMSPd increase prior to the melt period could be caused by the release of bottom-ice DMSPd, as well as the release and subsequent degradation of DMSPp-possessing ice algae in the upper water column (red dots on day 2 and 3; Fig. 3a). In late June, the simulated DMSPd concentrations increased up to about 6 nmol L^{-1} associated with the peak of simulated under-ice bloom (red line; Fig. 2b). This peak in simulated DMSPd was lower than the observed site-average value (ca. 11 nmol L^{-1}) from the second last sampling day. However, this observed site-average DMSPd value was associated with a large standard deviation

Biogeosciences Discuss., doi:10.5194/bg-2016-399, 2016
Manuscript under review for journal Biogeosciences
Published: 4 October 2016

because a single high value (ca. 30 nmol L^{-1}) was measured at 1.5 m depth, while values measured deeper in the water column were much lower ($\leq$ 3 nmol L^{-1}). Given this observed range, the simulated DMSPd peak is reasonable.

Figure 3c shows the simulated time series of the bottom-ice and the upper 10 m average DMS concentrations. The simulated bottom-ice DMS concentration increased gradually from April and reached about 1600 nmol L^{-1} in late May (black line; Fig. 3c). The timing of the simulated DMS peak lagged behind the simulated peaks of DMSPp and DMSPd by about one week. While no DMS observations were available to directly compare with the simulated DMS for this time period, the simulated DMS peak is close to the DMS concentration of 2000 nmol L^{-1} measured in the bottom ice in Resolute Passage at the end of the ice algal bloom in 2012 (Levasseur, 2013). The simulated bottom-ice DMS concentration remained close to its peak value until the beginning of June, then it quickly decreased to nearly 0 nmol L^{-1} by late June. In the water column, the simulated DMS concentrations increased gradually during early June and sharply during mid-June (red line; Fig. 3c). A few days after the simulated peaks of DMSPp and DMSPd in the upper water column, the simulated DMS reached its maximum value of about 9 nmol L^{-1} in late June.

3.1.4 Production and removal rates of DMSPd and DMS

The variability of the simulated DMSPd and DMS concentrations was driven by various physical and biogeochemical processes that are generally not well constrained by observations. Therefore, reporting the rates of those processes simulated by the model could help interpret the observed features. Figure 4a shows the individual terms in the production and removal rates of simulated bottom-ice DMSPd. Prior to mid-May, the simulated production rates by cell lysis and exudation increased to about 600 nmol L^{-1} d^{-1}, associated with the simulated ice algal bloom. However, the two rates differed by twofold during the peak of simulated ice algal bloom. The production rate by cell lysis exceeded 1200 nmol L^{-1} d^{-1} as a result of increased ice algal biomass as well as nutrient stress in the bottom ice. On the other hand, the production rate by exudation remained around 600 nmol L^{-1} d^{-1} because its potential enhancement due to nutrient stress was offset by reduced primary production. The removal of simulated bottom-ice DMSPd was dominated by bacterial consumption, while the contribution of free DMSP-lyase and flushing was minor. As parameterized in the model, the removal rate by bacterial consumption varied with the bottom-ice DMSPd concentration, and peaked at 1800 nmol L^{-1} d^{-1} in late May. The simulated removal rates by free DMSP-lyase and flushing were generally low with the former being at most 50 nmol L^{-1} d^{-1} in late May and the latter reaching about 80 nmol L^{-1} d^{-1} in mid-June. We note that the simulated removal rates by bacterial consumption and free DMSP-lyase both have the same functional form (Appendix A), and therefore the differences in these rates were a straightforward consequence of choices of parameter values.

Figure 4b shows the production and removal rates of simulated DMSPd in the uppermost layer (0.5 m below the ice) of the water column. In early June, the simulated production rates by flushing reached about 6 nmol L^{-1} d^{-1} and dominated the under-ice DMSPd budget as other terms were relatively small due to low biological activity under the ice. During the simulated under-ice phytoplankton bloom in mid-June, both cell lysis and exudation made similar contributions (27-28 nmol L^{-1} d^{-1}) to the DMSPd production in the uppermost layer of the water column, with the peak in cell lysis lagging a few days behind the peak in exudation. Finally, the simulated DMSPd production rates by sloppy feeding were negligible ($\leq$ 0.1 nmol L^{-1} d^{-1})

Biogeosciences Discuss., doi:10.5194/bg-2016-399, 2016
Manuscript under review for journal Biogeosciences
Published: 4 October 2016

due to low zooplankton biomass during the melt period. The removal of simulated DMSPd in the uppermost layer of the water column was governed by bacterial consumption, which increased up to 33 nmol L^{-1} d^{-1} during the under-ice bloom. The simulated DMSPd removal rates by bacterial consumption were comparable to the rates measured under the ice in Resolute Passage during the melt period in 2012 (3 to 44 nmol L^{-1} d^{-1}; Galindo et al., 2015). The simulated DMSPd removal rates by free DMSP-lyase were negligible (below 1 nmol L^{-1} d^{-1}) in the uppermost layer of the water column throughout the simulated period.

Figure 4c shows the production and removal rates of simulated bottom-ice DMS. The production of simulated bottom-ice DMS was dominated by bacterial DMSPd-to-DMS conversion, while the production by free DMSP-lyase was considerably less. As parameterized in the model, the temporal variability of DMS production rates by bacterial conversion resembled the temporal variability of DMSPd removal rates by bacterial consumption. The simulated DMS production rates by bacterial conversion were highest (ca. 350 nmol L^{-1} d^{-1}) during the peak of the ice algal bloom. The simulated DMS production rates by free DMSP-lyase increased gradually with the accumulation of DMSPd in the bottom ice (black line; Fig. 3b), but remained below 50 nmol L^{-1} d^{-1} throughout the simulated period. The removal of simulated DMS in the bottom ice was dominated by bacterial consumption, while photolysis and flushing became of comparable importance during the melt period. The simulated DMS removal rate by bacterial consumption reached about 325 nmol L^{-1} d^{-1} during the peak of ice algal bloom, balancing the DMS production by bacterial conversion. During the melt period, the simulated DMS removal rates by bacterial consumption were reduced due to a decrease in the bottom DMSPd (black line; Fig. 3b), while the removal rates by photolysis and flushing temporarily exceeded 50 nmol L^{-1} d^{-1}. The increase in the simulated DMS removal rates by photolysis at the beginning of the melt period was caused by the increased light penetration through the ice. Despite the continuous melting of simulated snow and ice and the enhancement in light penetration, the removal rate by photolysis decreased sharply after its peak in early June due to the decrease in the bottom-ice DMS concentrations (black line; Fig. 3c). In mid-June, the simulated DMS removal rate by flushing reached its peak that was quantitatively comparable to the rates by other simulated processes at that time.

Figure 4d shows the production and removal rates of simulated DMS in the uppermost layer of the water column. Similarly to the simulated under-ice DMSPd budget, the flushing of bottom-ice DMS dominated the under-ice DMS budget prior to the under-ice bloom. The simulated DMS production rates by flushing were comparable to the rates of other simulated processes associated with the under-ice bloom, and were at maximum (>5 nmol L^{-1} d^{-1}) in early June. During the same time period, the simulated DMS production rates by bacterial conversion were relatively low (0-1 nmol L^{-1} d^{-1}), which is consistent with the rates of 0-1.1 nmol L^{-1} d^{-1} measured in Resolute Passage during the initiation of the under-ice bloom in 2012 (Galindo et al., 2015). With the development of the under-ice boom, the simulated DMS production rates by bacterial conversion increased quickly and reached a peak of ca. 7 nmol L^{-1} d^{-1} in mid-June. The simulated DMS production by free DMSP-lyase had a negligible contribution (<0.2 nmol L^{-1} d^{-1}) throughout the simulation period. The removal process of DMS in the uppermost layer of the water column was dominated by bacterial consumption which increased up to ca. 6 nmol L^{-1} d^{-1} during the under-ice bloom. The simulated DMS removal rates by photolysis also increased during the same time period, but they were relatively low (ca. 1 nmol L^{-1} d^{-1}). Finally, it is important to note that, in the standard run, the loss of DMS by sea-to-air flux

Biogeosciences Discuss., doi:10.5194/bg-2016-399, 2016
Manuscript under review for journal Biogeosciences
Published: 4 October 2016

was prevented due to the presence of ice under the assumption that the surface was fully ice-covered throughout the simulation period. In Section 3.2.3, we will examine the effects of interstices in the ice on the simulated sea-to-air flux.

3.2 Sensitivity runs

3.2.1 Incorporation of sea-ice biogeochemistry

In the standard run, we showed that the flushing of the bottom-ice DMSPd and DMS respectively dominated the DMSPd and DMS budgets in the underlying water column prior to the onset of the under-ice phytoplankton bloom (Figs. 4b and 4d). To evaluate the changes in the simulated under-ice DMSPd and DMS concentrations due to this flushing, we conducted an additional simulation that excluded the sea-ice sulfur cycle module (NoIceSul) and compared the result with that of the standard run (Fig. 5 and Table 2). It should be emphasized that the sea-ice ecosystem module was still retained in this sensitivity run, hence the simulated ecosystem dynamics remained unchanged with respect to the standard run. The difference between the results of the two runs (Standard - NoIceSul) thus represents the impact of the sea-ice sulfur cycle. As expected, the exclusion of a sea-ice sulfur cycle resulted in a decrease in the under-ice DMSPd and DMS concentrations during most of the melt period. The differences in these concentrations between the two runs were most evident from 1 June to 25 June, with peak differences of 0.5 (DMSPd) and 2.1 nmol L^{-1} (DMS) appearing during the third week of June. Following 25 June, the concentration differences between the two runs became negligible, as the flushing became small toward the end of the melt period (Fig. 4). Over the simulation period, the incorporation of the sea-ice sulfur cycle resulted in 7 and 21 % increases in the respective under-ice DMSPd and DMS pools (Table 2). The increase in DMS was much greater than that of DMSPd because the flushing rates of DMS were relatively high among the under-ice DMS budget components, while the DMSPd flushing rates were smaller compared to the other under-ice DMSPd budget components considered in the model.

Besides the sea-ice sulfur cycle, it is possible that the incorporation of the sea-ice ecosystem itself can have an impact on the under-ice DMSPd and DMS concentrations. To examine this possibility, we conducted an additional simulation that excluded both the sea-ice sulfur cycle and ecosystem modules (NoIceBgc). It is clear from Fig. 5 that the under-ice DMSPd and DMS concentrations simulated in this run are significantly different from the results of the NoIceSul run, which implies a substantial contribution from the sea-ice ecosystem. In comparison to the NoIceSul run, the NoIceBgc run simulated the under-ice DMSPd and DMS concentrations that were higher in late June onward. The higher peaks in the under-ice DMSPd and DMS concentrations in the NoIceBgc run were associated with an under-ice phytoplankton bloom that was greater in magnitude than the bloom in the standard/NoIceSul run (Fig. 6a). The phytoplankton were able to increase biomass in the NoIceBgc run because of the heightened availability of nutrients in the absence of ice algae (Fig. 6b). Consequently, the production rates of DMSPd and DMS associated with this bloom were higher than those rates in the standard run, thereby yielding higher DMSPd and DMS concentrations under the ice in the NoIceBgc run. On the other hand, the under-ice DMSPd and DMS concentrations were lower in the NoIceBgc run than in the standard run prior to the emergence of their respective peaks in late June. These differences were again related to the difference in the phytoplankton biomass, which was also lower in the NoIceBgc run than in the standard run. Because a fraction of ice algal release is prescribed to enter the large phytoplankton pool in the model

Biogeosciences Discuss., doi:10.5194/bg-2016-399, 2016
Manuscript under review for journal Biogeosciences
Published: 4 October 2016

(Fig. 6c), the absence of ice algae in the NoIceBgc run lacked this seeding, resulting in lower phytoplankton biomass, as well as lower under-ice DMSPd and DMS concentrations prior to their peaks. Over the simulation period, the incorporation of sea-ice ecosystem resulted in a 16 % decrease in the under-ice DMS concentrations (Table 2). Hence, our results suggest that the incorporation of sea-ice ecosystem promotes the under-ice DMPd and DMS production by seeding the under-ice phytoplankton bloom, while it reduces the overall production by drawing down the available nutrients.

The results presented here suggest that the incorporation of sea-ice biogeochemistry (referring to both sea-ice sulfur cycle and ecosystem) has both direct and indirect effects on the under-ice DMSPd and DMS production. The direct effect is due to the incorporation of sea-ice sulfur cycle which increases the under-ice DMSPd and DMS concentrations through flushing from the bottom ice. The indirect effect is due to the incorporation of sea-ice ecosystem which, depending on the phase of the under-ice phytoplankton bloom, increases or decreases the the under-ice DMSPd and DMS concentrations by affecting the dynamics of the bloom. Over the simulation period, the incorporation of sea-ice biogeochemistry resulted in only a 2 % increase in the under-ice DMS concentrations, as the direct and indirect effects nearly counteracted each other (Table 2). However, the transient increases prior to the under-ice bloom peak (up to 5.6 nmol L^{-1}) could still be a significant source of episodic sea-air flux of DMS. We will examine the effects of these increases in the under-ice DMS production on the flux in Section 3.2.3.

3.2.2 Parameter uncertainty

The results of the standard run are influenced by the choice of uncertain model parameters. The model parameters of the sea-ice sulfur cycle are especially poorly constrained due to the scarcity of rate measurements within sea ice (Stefels et al., 2012). Therefore, it is important to report the sensitivity of our model results to changes in these parameters. We conducted five additional simulations to examine the respective changes in the simulated DMS concentrations in the bottom ice and underlying water column due to a doubling of the following five key parameters: intracellular DMSP:Chl a ratio (Case 1), DMS yield (Case 2), and rate constants for bacterial DMSPd consumption (Case 3), bacterial DMS consumption (Case 4), and photolysis (Case 5). Note that these parameter changes were applied only to the sea-ice sulfur cycle and not to the ocean sulfur cycle. We selected these five parameters considering that previous model sensitivity studies indicated their importance to marine sulfur cycle dynamics (Archer et al., 2004; Steiner and Denman, 2008) and that they are commonly measured parameters in the water column, therefore are expected to have better observational constraints in the future. Although the interannual field study in Resolute Passage indicated little variation (9.4-9.5) in the DMSP:Chl a ratio for ice algae (Galindo et al., 2014), other field measurements conducted in different regions found slightly lower (7.7; Kirst et al., 1991) and higher (ca. 20; Uzuka, 2003; Stefels et al., 2012) values. Furthermore, these reported values from earlier studies probably represent underestimates of the actual ratios in the natural environment due to anticipated DMSP loss associated with cell rupture during the melting process (Stefels et al., 2012). Given the observed range, the doubled ratio of 19 in Case 1 is reasonable in the natural environment. There has been only one study that measured the bottom-ice parameter values for Cases 2 and 4. In Case 2, the DMS yield fraction was increased to 40 %, which was the upper limit of the measured range for the bottom section of Antarctic ice core samples (Stefels et al., 2012). The doubled DMS consumption rate constant of 0.4 d^{-1} in Case 4 is within the range of 0.1-0.5 d^{-1} observed in the bottom ice of Antarctic sea ice (J. Stefels, University of Groningen, personal communication). To the best

Biogeosciences Discuss., doi:10.5194/bg-2016-399, 2016
Manuscript under review for journal Biogeosciences
Published: 4 October 2016

of our knowledge, no studies have measured the rate constants in the bottom ice considered in Cases 3 and 5. Doubling the values of these parameters is justified by the fact that the observed water column values of these parameters in the Arctic often differ by an order of magnitude (e.g., Luce et al., 2011; Galindo et al., 2015).

Figure 7 shows the simulated time series of bottom-ice and under-ice DMS concentrations in the standard and sensitivity runs. The results generally indicated that the parameter variations affected the magnitudes of the simulated DMS pools, while their temporal patterns remained similar to patterns in the standard run. Furthermore, the parameter variations generally had greater impacts on the bottom-ice DMS concentrations than on those in the underlying water column (Table 3). For example, doubling the intracellular DMSP:Chl a ratio (Case 1) and the DMS yield fraction (Case 2) resulted in doubling (100 % increase) and near-doubling (91 % increase) of the bottom-ice DMS, while the increases were lower (respectively 18 % and 13 %)in the uppermost layer of the water column. Nevertheless, doubling these parameters contributed the most to the change in the cumulative under-ice DMS among the five sensitivity runs. A previous model study by Lefèvre et al. (2002) also found these two parameters to be the most influential, and several other studies support the strong influence of variations in the intracellular DMSP:Chl a ratio (Gabric et al., 1993; Archer et al., 2004; Steiner and Denman, 2008). Doubling the remaining parameters (Cases 3-5) had relatively small effects (<10 %) on the cumulative under-ice DMS. This result indicates that field measurements targeting the two most sensitive parameters (i.e. DMSPp:Chl a ratio and DMS yield) will have the largest influence on constraining model-based estimates of sea-ice sulfur cycle processes.

To a certain extent, these sensitivities (e.g. sign and/or relative magnitude of the change in DMS) could have been predicted by recognizing from the model equations that doubling a single parameter results in doubling the DMS production or removal rate of a certain process either directly (Cases 2, 4, and 5) or indirectly (by doubling the production rate of precursor DMSPp; Case 1). The only exception was Case 3, in which doubling the bacterial DMSPd consumption rate constant affects both the production of DMS by bacterial conversion and the removal of DMSPd by bacterial consumption. Because the two processes have the opposite effect on the rate of change in DMS, it is even challenging to predict the sign (increase or decrease) of the change in DMS. The result of the sensitivity run indicated that the impact of doubling this parameter was a slight decrease (2 %) both in the bottom- and under-ice DMS pools, and therefore the increases in the rates of the two processes were almost balanced. Therefore, it is of particular importance to investigate the model sensitivity to variations in a parameter that has influence on multiple processes, such as the bacterial DMSPd consumption rate constant.

3.2.3 Sea-air DMS flux during the melt period

In the uppermost layer of the water column, the sea-air fluxes of DMS (μmol m^{-2} s^{-1}) were parameterized as a product of areal fraction of open water (f_{ow}), gas transfer velocity (k_{dms}), and the concentration of seawater DMS (DMS_{wc}):

$$Flux = f_{ow} k_{dms} DMS_{wc} \quad (1)$$

(2)

In the standard run, it was assumed that when sea ice was present, the surface was fully ice-covered and f_{ow} was set to zero. Although this assumption is reasonable when conducting simulations at a single point in space, it is less reasonable over an

Biogeosciences Discuss., doi:10.5194/bg-2016-399, 2016
Manuscript under review for journal Biogeosciences
Published: 4 October 2016

entire grid cell due to heterogeneity in the subgrid-scale structure of surface fields. In fact, as suggested by Levasseur et al. (1994), sea-air DMS fluxes can take place through openings in the ice (such as leads and cracks) and at the ice margin. Furthermore, laboratory, field, and model studies have suggested that fluxes of CO_2 through small scale areas of open water result in non-negligible fluxes in ice-covered regions (Loose et al., 2011; Else et al., 2012; Steiner et al., 2013). In order to quantify the potential emission of DMS through the open water in an ice-covered area, we conducted four additional standard runs with non-zero f_{ow} values (Table 4). In the first and second runs, the values of 0.02 and 0.1 were selected to represent small and large leads within the ice (Lindsay and Rothrock, 1995; Steiner et al., 2013). In the third run, the value of 0.5 was prescribed to represent either an extensive opening in the ice or emissions near the ice margin (such that only a half of under-ice DMS can be advected to the ice margin and make its way into the atmosphere). Finally in the fourth run, the value of 1 was assigned to represent emissions right at the ice margin. Note that these sensitivity runs are highly idealized (assumes partial or no ice cover for the emission, but full ice cover for the production), but provide some idea on the impacts of open-water fractions on the temporal variability of the DMS flux. Also, f_{ow} is included only in the DMS-flux parameterization, and has no influence on other physical or biogeochemical processes (such as surface heat fluxes). In order to evaluate the contribution of sea-ice biogeochemistry to the simulated flux, these four runs with non-zero f_{ow} values were also conducted for the NoIceSul and NoIceBgc cases.

During the melt period, observed winds were generally low to moderate, ranging on a daily average from 1 to <10 m s^{-1} (Fig. 8). However, occasional strong winds were also measured as indicated by daily maximum wind speeds exceeding 20 m s^{-1}. The time series of sea-air DMS fluxes simulated by the standard run using four different values of f_{ow} were generally high in late June, some of which coincided with these days of stronger winds as well as with peaks in under-ice DMS (Fig. 6b). In particular, the simulated fluxes were notably high on 16, 21, and 26 June, producing three distinct peaks in the time series. In the cases of emissions through partially open-water (f_{ow} = 0.02, 0.1, and 0.5), the simulated maximum fluxes (of up to 0.3, 1.2, and 4.9 μmol m^{-2} d^{-1}, respectively; Table 4) were higher than the observational upper-end flux estimates over regions of similar open-water fractions during July and August of 1994 (0.1 μmol m^{-2} d^{-1} for f_{ow} = 0.03-0.06 and 1.2 μmol m^{-2} d^{-1} for f_{ow} = 0.25-0.3; Sharma et al., 1999), most probably because these simulated maxima resulted partly from the peak in DMS associated with the under-ice bloom. In the cases of emissions near and at ice margins (f_{ow} = 0.5 and 1), the simulated maxima (of up to 4.9 and 8.1 μmol m^{-2} d^{-1}, respectively; Table 4) were comparable to the emissions under ice-free conditions estimated from previous oceanographic cruises in the Arctic (Leck and Persson, 1996; Sharma et al., 1999; Mungall et al., 2016). Furthermore, these simulated maxima exceeded the nucleation threshold of 2.5 μmol m^{-2} d^{-1}, above which the DMS flux has been suggested to be sufficiently high to promote new particle formation in pristine marine conditions (Pandis et al., 1994; Russell et al., 1994). It is also interesting to note that the simulated maxima do not scale linearly with the open-water fraction. Rather, there is evidence of saturation for these fluxes.

As expected, simulated sea-air fluxes were smaller in the NoIceSul run than in the standard run for each of the four f_{ow} values (Fig. 9b). The incorporation of sea-ice sulfur cycle affected the simulated fluxes most prominently during the first three weeks of June (Fig. 9d). The increase in the fluxes during this time period was due to the increase in the under-ice DMS through flushing as discussed in Section 3.2.1. This flux enhancement was particularly important during the first two weeks of June,

Biogeosciences Discuss., doi:10.5194/bg-2016-399, 2016
Manuscript under review for journal Biogeosciences
Published: 4 October 2016

during which the simulated fluxes would otherwise remain close to zero as shown in Fig. 9b. During the third week of June, the first and second simulated spikes in the flux time series were increased by as much as 1.9 μmol m^{-2} s^{-1} in the case of f_{ow} = 1 (Table 4). Overall, the incorporation of sea-ice sulfur cycle resulted in a 24-30 % DMS flux enhancement.

When both the sea-ice sulfur cycle and ecosystem modules were excluded from the model (NoIceBgc), the simulated flux time series fluctuated quite differently from those of the NoIceSul runs (Fig. 9c), implying an active contribution from sea-ice ecosystem to the simulated flux. The flux difference between the two runs indicates that the incorporation of sea-ice ecosystem results in an enhancement between 13 and 19 June, followed by a reduction from 19 June onward (Fig. 9e). The three simulated spikes in the flux time series of both the standard and NoIceSul runs were all affected by the incorporation of sea-ice ecosystem: the first spike was enhanced by as much as 4 μmol m^{-2} s^{-1} (in the case of f_{ow} = 1), while the second and third spikes were reduced by the similar amount. These changes in fluxes were primarily driven by the changes in under-ice DMS concentrations (Fig. 5b). Overall, the incorporation of sea-ice ecosystem resulted in a 7-13 % reduction in the simulated flux (Table 4).

Lastly, the overall effects of incorporating sea-ice biogeochemistry on simulated DMS fluxes were examined by calculating the flux difference between the standard and NoIceBgc runs (Fig. 9f). The largest positive flux difference occurring in the third week of June was due to the incorporation of both sea-ice sulfur cycle and ecosystem (Figs. 9d and e). This flux difference resulted in an enhancement of the first simulated spike by as much as 5.6 μmol m^{-2} s^{-1} (in the case of f_{ow} = 1). On the other hand, the largest negative flux difference coincided with the occurrance of the third simulated spike, resulting in a reduction in this spike by nearly 4 μmol m^{-2} s^{-1} (in the case of f_{ow} = 1). Over the simulation period, the incorporation of the sea-ice biogeochemistry resulted in a 8-20 % flux enhancement (Table 4). Considering that the overall enhancement of under-ice DMS concentrations due to the incorporation of sea-ice biogeochemistry was only 2 % (Section 3.2.1), this result demonstrates the potential importance of episodic fluxes (such as those spikes simulated in this study) to the cumulative DMS flux.

4 Conclusions

In the present study, we investigated the implications of sea-ice biogeochemistry for the oceanic production and emission of DMS in the Arctic. Our model results suggest that both sea-ice sulfur cycle and ecosystem have considerable impacts on the DMS production under the ice, and therefore should not be overlooked in the estimates of oceanic DMS fluxes. Specifically, sea-ice sulfur cycle enhanced the under-ice DMS production directly by the flushing of bottom-ice DMSPd and DMS into the underlying water column, while the production was enhanced as well as reduced by the sea-ice ecosystem at various phases of the under-ice phytoplankton bloom. In the case of first-year landfast ice in Resolute Passage, we estimated that the incorporation of sea-ice sulfur cycle resulted in a 21 % enhancement of DMS concentrations under the ice and a 24-30 % enhancement of sea-air DMS fluxes during the melt period. In contrast, the incorporation of a sea-ice ecosystem resulted in an overall reduction in the under-ice DMS production (16 %) as well as its emission towards the atmosphere (7-13 %). However, the overall effect of sea-ice biogeochemistry (i.e. both sulfur cycle and ecosystem) appears to be an enhancement for both the DMS production (2 %) and emission (8-20 %). Furthermore, in the vicinity of ice margins, the simulated spikes in sea-air fluxes of DMS originating from the bottom ice and underlying water column were comparable to some of the local

Biogeosciences Discuss., doi:10.5194/bg-2016-399, 2016
Manuscript under review for journal Biogeosciences
Published: 4 October 2016

maxima in the summertime flux estimated for ice-free waters in the Arctic. We acknowledge the simplified representation of complex reality of the sea-ice sulfur cycle dynamics considered in our model, and note that the results of model simulations are subject to uncertainty owing to uncertainties in the model parameters and parameterizations. Furthermore, our model results are representative for a particular year, location, and specific environmental conditions, hence the values presented here could be different under alternative circumstances. One possible suggestion for future model development is to incorporate the state dependence of bacterial parameters that are deemed influential to the sea-ice sulfur cycle dynamics, such as the bacterial DMS yield fraction.

To improve model-based estimates of oceanic DMS emissions in the Arctic under present-day and future climates, we make the following recommendations for future studies: both the sea-ice sulfur cycle and ecosystem should be incorporated into model simulations at a regional (pan-Arctic) scale; and more field measurements, especially of rates, in the sea ice should be conducted to further refine the representation of key processes. Ultimately, ocean circulation models incorporating both the sea-ice sulfur cycle and ecosystem should be coupled to atmospheric chemistry transport models in order to explore the possibility of regional climate regulation by oceanic DMS emissions within the Arctic.

Appendix A: Detailed model description

The set of differential equations describing the temporal evolution of DMSPp, DMSPd, and DMS in the bottom ice and water column is provided below. The list of variables and parameters involved in the model is provided in Table 1.

A1 Sea-ice sulfur cycle

The concentration (nmol L^{-1}) of the particulate phase of DMSP in the bottom ice ($DMSPp$) is simulated diagnostically by assuming a fixed DMSPp-to-chlorophyll a intracellular ratio (nmol S:μg Chl a) for ice algae (q):

$$\frac{\partial}{\partial t}\left(DMSPp\right) = q\frac{\partial}{\partial t}\left(IA\right) \tag{A1}$$

where IA is the ice algal biomass (μg Chl a L^{-1}). The intracellular ratio varies among algal species (Keller, 1989; Matrai and Keller, 1994) and also varies with various abiotic factors including temperature (Karsten et al., 1992; van Rijssel and Gieskes, 2002), salinity (Karsten et al., 1992), light (Karsten et al., 1992; Stefels and van Leeuwe, 1998; Sunda et al., 2002; Archer et al., 2009; Galindo et al., 2016) and nutrients (Stefels and van Leeuwe, 1998; Sunda et al., 2007; Archer et al., 2009). The reported values for q vary from 7.7 (Kirst et al., 1991) to about 20 (Uzuka, 2003; Stefels et al., 2012). Values of 9.4-9.5 have been reported for Resolute Passage (Galindo et al., 2014). In the standard run, we set q to 9.5 nmol S:μg Chl a.

The concentration (nmol L^{-1}) of the dissolved phase of DMSP in the bottom ice ($DMSPd$) is simulated prognostically:

$$\begin{aligned}\frac{\partial}{\partial t}\left(DMSPd\right) = {} & F_{lysis} + F_{exudation} \\ & - F^{dmspd}_{consumption} - F_{free} - F^{dmspd}_{flushing}\end{aligned} \tag{A2}$$

Biogeosciences Discuss., doi:10.5194/bg-2016-399, 2016
Manuscript under review for journal Biogeosciences
Published: 4 October 2016

where F denotes the production or removal rate (nmol L^{-1} d^{-1}) for each of the processes considered in the model (Fig. 1). The first two terms in Eq. (A2) represent the production rates of bottom-ice DMSPd by cell lysis and exudation, respectively. Following Archer et al. (2004), these processes are parameterized to increase under nutrient stress:

$$F_{lysis} = \frac{1}{L_{nut} + 0.1} k_{lysis} DMSPp \tag{A3}$$

$$F_{exudation} = [f_{active} + (1 - f_{active})(1 - L_{nut})]\,\mu DMSPp \tag{A4}$$

where L_{nut} represents the nutrient limitation index (-) for ice algal growth, k_{lysis} represents the rate constant (d^{-1}) for cell lysis, f_{active} represents the active exudation fraction (-), and μ represents the ice algal specific growth rate (d^{-1}). Both L_{nut} and μ are calculated by the ecosystem module. The two parameters involving cell lysis (k_{lysis}) and exudation (f_{active}) are generally poorly constrained in the sulfur cycle models because the measurements of production rates of DMSPd by cell lysis and exudation are very limited in seawater (Laroche et al., 1999). To our best knowledge, these rates have not been measured within sea ice. In the standard run, k_{lysis} and f_{active} are respectively set to 0.03 d^{-1} and 0.05, which are similar to the values used in previous ocean sulfur cycle models (Archer et al., 2004; Steiner and Denman, 2008).

The third term in Eq. (A2) represents the removal rate of bottom-ice DMSPd by bacterial consumption. DMSPd is an important source of carbon and sulfur for bacteria in the marine environment, as the bacterial consumption of DMSPd can account for up to 15 % of their total carbon demand and almost all of their sulfur demand (Stefels et al., 2007). In the model, this removal process is parameterized as:

$$F^{dmspd}_{consumption} = k_{dmspd} DMSPd \tag{A5}$$

where k_{dmspd} represents the rate constant (d^{-1}) for bacterial consumption of DMSPd. There are no reported values for k_{dmspd} in sea ice. In the standard run, k_{dmspd} is set to 1 d^{-1} based on the model calibration.

The fourth term in Eq. (A2) (F_{free}) represents the removal rate of DMSPd by free DMSP-lyase present in the bottom ice. This process is parameterized as the product of a rate constant (k_{free} [d^{-1}]) and the concentration of bottom-ice DMSPd:

$$F_{free} = k_{free} DMSPd \tag{A6}$$

In previous model studies, this process was considered as a minor removal pathway of DMSPd with k_{free} varying from 0.01 d^{-1} (Archer et al., 2004) to 0.04 d^{-1} (Steiner et al., 2006). In the standard run, k_{free} is set to 0.02 d^{-1}.

The fifth term in Eq. (A2) ($F^{dmspd}_{flushing}$) represents the removal rate of DMSPd via flushing which results in the release of bottom-ice DMSPd into the water column. In the model, this process is parameterized to be proportional to the flushing rate ($R_{flushing}$ [d^{-1}]):

$$F^{dmspd}_{flushing} = R_{flushing} DMSPd \tag{A7}$$

$R_{flushing}$ is determined by the physical model which accounts for both the percolation of snow meltwater and the melting of the ice (Mortenson et al., Submitted).

Biogeosciences Discuss., doi:10.5194/bg-2016-399, 2016
Manuscript under review for journal Biogeosciences
Published: 4 October 2016

The concentration (nmol L^{-1}) of DMS in the bottom ice (DMS) is simulated prognostically:

$$\frac{\partial}{\partial t}(DMS) = F_{conversion} + F^{dms}_{free} - F^{dms}_{consumption} - F_{photolysis} - F^{dms}_{flushing} \tag{A8}$$

The first term in Eq. (A8) ($F_{conversion}$) represents the production rate of bottom-ice DMS by bacterial conversion of DMSPd to DMS. This process is one of the two major degradation pathways for DMSPd consumed by bacteria in open waters. The bacteria cleave DMSPd and yield DMS along with other products such as acrylate and a proton (Stefels et al., 2007). The other major degradation pathway is known as demethylation/demethiolation (Kiene and Linn, 2000), which is accounted for in the model as part of the DMSPd removal rate by bacterial consumption. The rate of DMS production via bacterial DMSPd conversion is often scaled to the bacterial consumption rate of DMSPd, such that the former can be expressed as a fraction of the latter:

$$F_{conversion} = f_{yield} F^{dmspd}_{consumption} \tag{A9}$$

where f_{yield} is known as the DMS yield fraction (-). Only one study has reported values for f_{yield} measured in the bottom ice, all less than 0.4 (Stefels et al., 2012). In the standard run, f_{yield} is set to 0.2.

The second term in Eq. (A8) (F_{free}) represents the production rate of bottom-ice DMS via free DMSP-lyase which is equivalent to the fourth term in Eq. (A2) and is defined in Eq. (A6).

The third term in Eq. (A8) ($F^{dms}_{consumption}$) represents the removal rate of bottom-ice DMS by bacterial consumption which is parameterized similarly to the bacterial consumption of bottom-ice DMSPd (Eq. (A5)):

$$F^{dms}_{consumption} = k_{dms} DMS \tag{A10}$$

where k_{dms} represents the rate constant (d^{-1}) for bacterial consumption of DMS. The only measurements of k_{dms} conducted for ice core samples showed a range from 0.1 to 0.5 d^{-1} for the bottom ice (J. Stefels, University of Groningen, personal communication). In the standard run, k_{dms} is set to 0.2 d^{-1}.

The fourth term in Eq. (A8) ($F_{photolysis}$) represents the removal rate of bottom-ice DMS by photolysis, a photochemical process that converts DMS into its oxidation product, DMSO. The rate of photolysis is primarily determined by ambient light conditions, particularly in the ultraviolet (UV) wavelengths (Toole et al., 2004). However, we do not incorporate the UV dependence on the photlysis parameterization as the model does not have a representation for UV. Instead, we parameterize the light dependence of $F_{photolysis}$ using the photosynthetically active radiation similarly to Archer et al. (2004):

$$F_{photolysis} = k_{photolysis} \frac{PAR}{PAR + h_{photolysis}} DMS \tag{A11}$$

where PAR represents the photosynthetically active radiation reaching the bottom ice (W m^{-2}), which is computed by the physical model. The parameters, $k_{photolysis}$ and $h_{photolysis}$ represent the rate constant (d^{-1}) and the half-saturation constant (W m^{-2}) for photolysis in the bottom ice. To the best of our knowledge, no studies have reported the values for photolysis rate constant in the bottom ice. In the standard run, $k_{photolysis}$ is set to 0.1 d^{-1} based on the measurements in the water column

Biogeosciences Discuss., doi:10.5194/bg-2016-399, 2016
Manuscript under review for journal Biogeosciences
Published: 4 October 2016

(discussed in Sec. A2). We assume that photolysis is inhibited under low light conditions, and therefore set $h_{photolysis}$ to 1 W m^{-2}.

The last term in Eq. (A8) ($F^{dms}_{flushing}$) represents the removal rate of bottom-ice DMS due to flushing, which is parameterized in the same way as $F^{dmspd}_{flushing}$:

$$F^{dms}_{flushing} = R_{flushing} DMS \tag{A12}$$

A2 Ocean sulfur cycle

The concentration (nmol L^{-1}) of particulate DMSP in the water column ($DMSPp_{wc}$) is simulated diagnostically by assuming a fixed DMSPp-to-chlorophyll a intracellular ratio (nmol S:μg Chl a) for each phytoplankton group (q_{p1} and q_{p2}):

$$\frac{\partial}{\partial t}\left(DMSPp_{wc}\right) = q_{p1}\frac{\partial}{\partial t}P1 + q_{p2}\frac{\partial}{\partial t}P2 \tag{A13}$$

where $P1$ and $P2$ represent the biomass of small and large phytoplankton (μg Chl a L^{-1}), respectively. Although the model does not specify the species group for $P1$, it is assumed that $P1$ produces more DMSP for a given amount of chlorophyll a than diatoms ($P2$). In the standard run, q_{p1} is set to 100 which is close to the intracellular ratios for non-diatom species groups reported in Stefels et al. (2007), and q_{p2} is set to 9.5 which is equivalent to the intracellular ratio for ice algae (q).

The concentration (nmol L^{-1}) of DMSPd in the water column ($DMSPd_{wc}$) is simulated prognostically:

$$\frac{\partial}{\partial t}\left(DMSPd_{wc}\right) = F^{wc}_{lysis} + F^{wc}_{exudation} + F^{wc}_{sloppy} + F^{dmspd.wc}_{flushing} - F^{dmspd.wc}_{consumption} - F^{wc}_{free} + \frac{\partial}{\partial z}\left(K_z \frac{\partial}{\partial z}\left(DMSPd_{wc}\right)\right) \tag{A14}$$

where the last term represents the mixing rate of DMSPd between model layers, with K_z being the vertical eddy diffusivity ($m^2 s^{-1}$) which is calculated by the ocean physical model.

The first, second, fifth, and sixth terms in Eq. (A14) (F^{wc}_{lysis}, $F^{wc}_{exudation}$, $F^{dmspd.wc}_{consumption}$, F^{wc}_{free}) are parameterized similarly to those in the sea-ice sulfur cycle (Eq. (A2)):

$$F^{wc}_{lysis} = \frac{1}{L^{p1}_{nut} + 0.1} k^{p1}_{lysis} q_{p1} P1 + \frac{1}{L^{p2}_{nut} + 0.1} k^{p2}_{lysis} q_{p2} P2 \tag{A15}$$

$$F^{wc}_{exudation} = \left[f^{p1}_{active} + \left(1 - f^{p1}_{active}\right)\left(1 - L^{p1}_{nut}\right)\right]\mu_{p1} q_{p1} P1 + \left[f^{p2}_{active} + \left(1 - f^{p2}_{active}\right)\left(1 - L^{p2}_{nut}\right)\right]\mu_{p2} q_{p2} P2 \tag{A16}$$

$$F^{dmspd.wc}_{consumption} = k^{wc}_{dmspd} DMSPd_{wc} \tag{A17}$$

$$F^{wc}_{free} = k^{wc}_{free} DMSPd_{wc} \tag{A18}$$

where the nutrient limitation indices (L^{p1}_{nut} and L^{p2}_{nut}) and the growth rates (μ_{p1} and μ_{p2}) of small and large phytoplankton, respectively, are calculated by the ocean ecosystem module. To our best knowledge, there are no reported values for the cell lysis rate constants (k^{p1}_{lysis} and k^{p2}_{lysis}) and the active exudation fractions (f^{p1}_{active} and f^{p2}_{active}) in ice-covered regions. In the standard run, k^{p1}_{lysis} and k^{p2}_{lysis} are set to 0.03 d^{-1}, and f^{p1}_{active} and f^{p2}_{active} are set to 0.05 for both small and large phytoplankton. k^{wc}_{dmspd} represents the bacterial DMSPd consumption rate constant in the water column. The reported values for k^{wc}_{dmspd} in Arctic

Biogeosciences Discuss., doi:10.5194/bg-2016-399, 2016
Manuscript under review for journal Biogeosciences
Published: 4 October 2016

surface water vary from 1.5 d^{-1} during autumn (Luce et al., 2011; Motard-Côté et al., 2012) to 4.1 d^{-1} during spring (Galindo et al., 2015). In the standard run, k^{wc}_{dmspd} is set to 5 d^{-1}) based on the model calibration. k^{wc}_{free} represents the rate constant for free DMSP-lyase in the water column, which is set to 0.02 d^{-1} in the standard run.

The third term in Eq. (A14) represents the production rate of DMSPd in the water column by sloppy feeding:

$$F_{sloppy} = f^{z1}_{sloppy} q_{p1} R^{z1}_{p1} + f^{z2}_{sloppy} q_{p2} R^{z2}_{p2} \tag{A19}$$

where f^{z1}_{sloppy} and f^{z2}_{sloppy} represent the fractions of sloppy feeding by small and large zooplankton. In the standard run, these fractions are set to 0.3 for both zooplankton groups, based on the findings that 20 to 70 % of grazed DMSPp is released into the ambient seawater as DMSPd (Stefels et al., 2007). R^{z1}_{p1} and R^{z2}_{p2} represent the loss rates (μg Chl a L^{-1} d^{-1}) of small and large phytoplankton due to grazing by small and large zooplankton, respectively, which are calculated by the ecosystem module.

The fourth term in Eq. (A14) represents the flushing rate of DMSPd, which can be written in the vertically discretized form as:

$$F^{dmspd.wc}_{flushing} = F^{dmspd}_{flushing} \frac{h_{bi}}{h_{z_0}} \delta_{z,z_0} \tag{A20}$$

where h_{bi} and h_{z_0} are the thicknesses (m) of the bottom ice and uppermost layer of the water column, respectively. The Kronecker's delta (δ_{z,z_0}) equals 1 at the uppermost layer of the water column (z_0), whereas it is 0 elsewhere.

The concentration (nmol L^{-1}) of DMS in the water column (DMS_{wc}) is simulated prognostically:

$$\frac{\partial}{\partial t}(DMS_{wc}) = F^{wc}_{conversion} + F^{wc}_{free} + F^{dms.wc}_{flushing} - F^{dms.wc}_{consumption} - F^{wc}_{photolysis} - F_{seaair} + \frac{\partial}{\partial z}\left(K_z \frac{\partial}{\partial z}(DMS_{wc})\right) \tag{A21}$$

where the last term represents the mixing of DMS between model layers, as described for the mixing rate of DMSPd.

The first, fourth, and fifth terms in Eq. (A21) respectively represent the DMS production rate by bacterial conversion ($F^{wc}_{conversion}$), the DMS removal rates by bacterial consumption ($F^{dms.wc}_{consumption}$) and photolysis ($F^{wc}_{photolysis}$) in the water column, which are parameterized similarly to those in the bottom ice:

$$F^{wc}_{conversion} = f^{wc}_{yield} k^{wc}_{dmspd} DMSPd_{wc} \tag{A22}$$

$$F^{dms.wc}_{consumption} = k^{wc}_{dms} DMS_{wc} \tag{A23}$$

$$F^{wc}_{photolysis} = k^{wc}_{photolysis} \frac{PAR_{wc}}{PAR_{wc} + h^{wc}_{photolysis}} DMS_{wc} \tag{A24}$$

where f^{wc}_{yield}, k^{wc}_{dms}, $k^{wc}_{photolysis}$, and $h^{wc}_{photolysis}$ respectively represent the DMS yield fraction (-), the bacterial DMS consumption rate constant (d^{-1}), and the rate constant (d^{-1}) and the half-saturation constant (W m^{-2}) for photolysis in the water column. The reported values for f^{wc}_{yield} are highly variable (0.05-1) in temperate water (Simo and Pedros-Alio, 1999) and moderately variable (0.04-0.3) in Arctic water (Luce et al., 2011; Motard-Côté et al., 2012). The only DMS yield fraction measurements available for the under-ice water column reported low values with relatively small range (0.02-0.1) as the measurements were conducted prior to the under-ice phytoplankton bloom (Galindo et al., 2015). In the standard run, f^{wc}_{yield} is set to 0.2. The reported values for k^{wc}_{dms} in Arctic surface water vary from 0.05 to 1.00 (mean of 0.17) d^{-1} for the Canadian High

Biogeosciences Discuss., doi:10.5194/bg-2016-399, 2016
Manuscript under review for journal Biogeosciences
Published: 4 October 2016

Arctic in October (Luce et al., 2011) and from 0.14 and 2.2 (mean of 0.9) d^{-1} for the Greenland Sea (Gali and Simo, 2010) in July. In the standard run, k_{dms}^{wc} is set to 0.2 d^{-1}. The reported range of $k_{photolysis}^{wc}$ measured in Arctic water during the summer varies from 0.01-0.11 d^{-1} for the Bering Sea (Deal et al., 2005) and the Canadian Arctic (Taalba et al., 2012) to 0.23-1.05 d^{-1} for the Greenland sea (Gali and Simo, 2010). In the standard run, $k_{photolysis}^{wc}$ is set to 0.1 d^{-1} and $h_{photolysis}^{wc}$ is set to 1 W m^{-2}.

The third term in Eq. (A21) represents the flushing rate of DMS, which can be written in the vertically discretized form as:

$$F_{flushing}^{dms.wc} = F_{flushing}^{dms} \frac{h_{bi}}{h_{z_0}} \delta_{z,z_0} \tag{A25}$$

Finally, the sixth term in Eq. (A21) represents the removal rate (nmol L^{-1} d^{-1}) of DMS in the uppermost layer of the water column by the sea-to-air fluxes, which can be written in the vertically discretized form as:

$$F_{seaair} = f_{ow} \frac{k_{dms} DMS_{wc}}{h_{z_0}} \delta_{z,z_0} \tag{A26}$$

where f_{ow} represents the fraction (-) of open water to account for fluxes through a partially ice-covered surface. In the standard run, f_{ow} is set to 0 in the presence of sea ice, which is assumed to completely block the air-sea DMS fluxes. k_{dms} represents the gas transfer velocity (m s^{-1}) for DMS. Although previous flux measurements of DMS based on the eddy covariance technique suggest that, under low to moderate winds, the gas transfer velocity can be reasonably predicted by assuming a linear wind-speed dependence (Huebert et al., 2010; Goddijn-Murphy et al., 2012; Bell et al., 2013, 2015), a recent study reconciling the eddy covariance technique with the dual tracer technique suggests that the linear wind-only-based parameterization will likely underestimate the gas transfer velocity under strong winds due to the enhancement of the bubble-mediated transfer (Goddijn-Murphy et al., 2015). In this study, the gas transfer velocity is parameterized based on Nightingale et al. (2000), which assumes a combination of linear and quadratic dependence on wind speed. Although this parameterization does not represent the bubble-mediated transfer, the gas transfer velocities predicted by this parameterization were, among other "wind speed only" parameterizations, closest to the prediction by the hybrid model of Goddijn-Murphy et al. (2015). The gas transfer velocity parameterization of Nightingale et al. (2000) was normalized to a Schmidt nubmer of 600 (k_{600}), and therefore, was corrected to a Schmidt number of DMS (Sc_{dms}) at a given temperature of ambient seawater (T_{z_0} in $^{\circ}C$) in the uppermost layer of the water column based on Saltzman et al. (1993):

$$k_{dms} = k_{600} \left(\frac{Sc}{600} \right)^{-1/2} \tag{A27}$$

$$k_{600} = 0.333 U_{10} + 0.222 U_{10}^2 \tag{A28}$$

$$Sc_{dms} = 2674 - 147.12 T_{z_0} + 3.726 T_{z_0}^2 - 0.038 T_{z_0}^3 \tag{A29}$$

where U_{10} is the observed wind speed at 10 m (m s^{-1}).

Acknowledgements. This study contributes to the SCOR Working group on Biogeochemical Exchange Processes at Sea Ice Interfaces (BEPSII), the Network on Climate and Aerosols: Addressing Key Uncertainties in Remote Canadian Environments (NETCARE), and ArcticNet. NS is supported by Fisheries and Oceans Canada. AHM acknowledges support from the Natural Sciences and Engineering Research Council

Biogeosciences Discuss., doi:10.5194/bg-2016-399, 2016
Manuscript under review for journal Biogeosciences
Published: 4 October 2016

of Canada. The restoration data for temperature, salinity, and velocity fields in the water column were provided by Xianmin Hu (University of Alberta).

Biogeosciences Discuss., doi:10.5194/bg-2016-399, 2016
Manuscript under review for journal Biogeosciences
Published: 4 October 2016

References

Abraham, C., Steiner, N., Monahan, A., and Michel, C.: Effects of subgrid-scale snow thickness variability on radiative transfer in sea ice, Journal of Geophysical Research: Oceans, pp. n/a–n/a, doi:10.1002/2015JC010741, http://onlinelibrary.wiley.com/doi/10.1002/2015JC010741/abstract, 2015.

Alcolombri, U., Ben-Dor, S., Feldmesser, E., Levin, Y., Tawfik, D. S., and Vardi, A.: Identification of the algal dimethyl sulfide–releasing enzyme: A missing link in the marine sulfur cycle, Science, 348, 1466–1469, doi:10.1126/science.aab1586, http://www.sciencemag.org/content/348/6242/1466, 2015.

Archer, S., Cummings, D., Llewellyn, C., and Fishwick, J.: Phytoplankton taxa, irradiance and nutrient availability determine the seasonal cycle of DMSP in temperate shelf seas, Marine Ecology Progress Series, 394, 111–124, doi:10.3354/meps08284, http://www.int-res.com/abstracts/meps/v394/p111-124/, 2009.

Archer, S. D., Gilbert, F. J., Allen, J. I., Blackford, J., and Nightingale, P. D.: Modelling of the seasonal patterns of dimethylsulphide production and fate during 1989 at a site in the North Sea, Canadian Journal of Fisheries and Aquatic Sciences, 61, 765–787, doi:10.1139/f04-028, http://www.nrcresearchpress.com/doi/abs/10.1139/f04-028, 2004.

Asher, E. C., Dacey, J. W. H., Mills, M. M., Arrigo, K. R., and Tortell, P. D.: High concentrations and turnover rates of DMS, DMSP and DMSO in Antarctic sea ice, Geophysical Research Letters, 38, L23 609, doi:10.1029/2011GL049712, http://onlinelibrary.wiley.com/doi/10.1029/2011GL049712/abstract, 2011.

Bates, T. S., Lamb, B. K., Guenther, A., Dignon, J., and Stoiber, R. E.: Sulfur emissions to the atmosphere from natural sourees, Journal of Atmospheric Chemistry, 14, 315–337, doi:10.1007/BF00115242, http://link.springer.com.ezproxy.library.uvic.ca/article/10.1007/BF00115242, 2004.

Bell, T. G., De Bruyn, W., Miller, S. D., Ward, B., Christensen, K., and Saltzman, E. S.: Air–sea dimethylsulfide (DMS) gas transfer in the North Atlantic: evidence for limited interfacial gas exchange at high wind speed, Atmospheric Chemistry and Physics, 13, 11 073–11 087, doi:10.5194/acp-13-11073-2013, http://www.atmos-chem-phys.net/13/11073/2013/, 2013.

Bell, T. G., De Bruyn, W., Marandino, C. A., Miller, S. D., Law, C. S., Smith, M. J., and Saltzman, E. S.: Dimethylsulfide gas transfer coefficients from algal blooms in the Southern Ocean, Atmos. Chem. Phys., 15, 1783–1794, doi:10.5194/acp-15-1783-2015, http://www.atmos-chem-phys.net/15/1783/2015/, 2015.

Burchard, H., Bolding, K., and Villarreal, M. R.: GOTM, a general ocean turbulence model: Theory, implementation and test cases, Space Applications Institute, 1999.

Burchard, H., Bolding, K., Kühn, W., Meister, A., Neumann, T., and Umlauf, L.: Description of a flexible and extendable physical–biogeochemical model system for the water column, Journal of Marine Systems, 61, 180–211, doi:10.1016/j.jmarsys.2005.04.011, http://www.sciencedirect.com/science/article/pii/S0924796306000248, 2006.

Chang, R. Y.-W., Sjostedt, S. J., Pierce, J. R., Papakyriakou, T. N., Scarratt, M. G., Michaud, S., Levasseur, M., Leaitch, W. R., and Abbatt, J. P. D.: Relating atmospheric and oceanic DMS levels to particle nucleation events in the Canadian Arctic, Journal of Geophysical Research, 116, doi:10.1029/2011JD015926, http://doi.wiley.com/10.1029/2011JD015926, 2011.

Charlson, R. J., Lovelock, J. E., Andreae, M. O., and Warren, S. G.: Oceanic phytoplankton, atmospheric sulphur, cloud albedo and climate, Nature, 326, 655–661, doi:10.1038/326655a0, http://www.nature.com/nature/journal/v326/n6114/abs/326655a0.html, 1987.

Deal, C. J., Kieber, D. J., Toole, D. A., Stamnes, K., Jiang, S., and Uzuka, N.: Dimethylsulfide photolysis rates and apparent quantum yields in Bering Sea seawater, Continental Shelf Research, 25, 1825–1835, doi:10.1016/j.csr.2005.06.006, http://linkinghub.elsevier.com/retrieve/pii/S0278434305001196, 2005.

Dukhovskoy, D. S., Myers, P. G., Platov, G., Timmermans, M.-L., Curry, B., Proshutinsky, A., Bamber, J. L., Chassignet, E., Hu, X., Lee, C. M., and Somavilla, R.: Greenland freshwater pathways in the sub-Arctic Seas from model experiments with passive tracers, Journal of Geophysical Research: Oceans, 121, 877–907, doi:10.1002/2015JC011290, http://onlinelibrary.wiley.com/doi/10.1002/2015JC011290/abstract, 2016.

Elliott, S., Deal, C., Humphries, G., Hunke, E., Jeffery, N., Jin, M., Levasseur, M., and Stefels, J.: Pan-Arctic simulation of coupled nutrient-sulfur cycling due to sea ice biology: Preliminary results, Journal of Geophysical Research, 117, doi:10.1029/2011JG001649, http://doi.wiley.com/10.1029/2011JG001649, 2012.

Else, B. G. T., Papakyriakou, T. N., Galley, R. J., Mucci, A., Gosselin, M., Miller, L. A., Shadwick, E. H., and Thomas, H.: Annual cycles of pCO2sw in the southeastern Beaufort Sea: New understandings of air-sea CO2 exchange in arctic polynya regions: ANNUAL pCO2sw CYCLE IN POLYNYA REGIONS, Journal of Geophysical Research: Oceans, 117, n/a–n/a, doi:10.1029/2011JC007346, http://doi.wiley.com/10.1029/2011JC007346, 2012.

Flato, G. M. and Brown, R. D.: Variability and climate sensitivity of landfast Arctic sea ice, Journal of Geophysical Research: Oceans, 101, 25 767–25 777, doi:10.1029/96JC02431, http://onlinelibrary.wiley.com.ezproxy.library.uvic.ca/doi/10.1029/96JC02431/abstract, 1996.

Gabric, A., Murray, N., Stone, L., and Kohl, M.: Modelling the production of dimethylsulfide during a phytoplankton bloom, Journal of Geophysical Research: Oceans (1978–2012), 98, 22 805–22 816, http://onlinelibrary.wiley.com/doi/10.1029/93JC01773/full, 1993.

Gali, M. and Simo, R.: Occurrence and cycling of dimethylated sulfur compounds in the Arctic during summer receding of the ice edge, Marine Chemistry, 122, 105–117, doi:10.1016/j.marchem.2010.07.003, http://linkinghub.elsevier.com/retrieve/pii/S0304420310000861, 2010.

Galindo, V., Levasseur, M., Mundy, C., Gosselin, M., Tremblay, J.-E., Scarratt, M., Gratton, Y., Papakiriakou, T., Poulin, M., and Lizotte, M.: Biological and physical processes influencing sea ice, under-ice algae, and dimethylsulfoniopropionate during spring in the Canadian Arctic Archipelago, Journal of Geophysical Research: Oceans, doi:10.1002/2013JC009497, http://onlinelibrary.wiley.com/doi/10.1002/2013JC009497/abstract, 2014.

Galindo, V., Levasseur, M., Scarratt, M., Mundy, C., Gosselin, M., Kiene, R., Gourdal, M., and Lizotte, M.: Under-ice microbial dimethylsulfoniopropionate metabolism during the melt period in the Canadian Arctic Archipelago, Marine Ecology Progress Series, 524, 39–53, doi:10.3354/meps11144, http://www.int-res.com/abstracts/meps/v524/p39-53/, 2015.

Galindo, V., Levasseur, M., Mundy, C. J., Gosselin, M., Scarratt, M., Papakyriakou, T., Stefels, J., Gale, M. A., Tremblay, J.-E., and Lizotte, M.: Contrasted sensitivity of DMSP production to high light exposure in two Arctic under-ice blooms, Journal of Experimental Marine Biology and Ecology, 475, 38–48, doi:10.1016/j.jembe.2015.11.009, http://linkinghub.elsevier.com/retrieve/pii/S0022098115300599, 2016.

Goddijn-Murphy, L., Woolf, D. K., and Marandino, C.: Space-based retrievals of air-sea gas transfer velocities using altimeters: Calibration for dimethyl sulfide, Journal of Geophysical Research: Oceans, 117, C08 028, doi:10.1029/2011JC007535, http://onlinelibrary.wiley.com.ezproxy.library.uvic.ca/doi/10.1029/2011JC007535/abstract, 2012.

Goddijn-Murphy, L., Woolf, D. K., Callaghan, A. H., Nightingale, P. D., and Shutler, J. D.: A reconciliation of empirical and mechanistic models of the air-sea gas transfer velocity, Journal of Geophysical Research: Oceans, pp. n/a–n/a, doi:10.1002/2015JC011096, http://doi.wiley.com/10.1002/2015JC011096, 2015.

Huebert, B. J., Blomquist, B. W., Yang, M. X., Archer, S. D., Nightingale, P. D., Yelland, M. J., Stephens, J., Pascal, R. W., and Moat, B. I.: Linearity of DMS transfer coefficient with both friction velocity and wind speed in the moderate wind speed range, Geophysical Research Letters, 37, L01 605, doi:10.1029/2009GL041203, http://onlinelibrary.wiley.com.ezproxy.library.uvic.ca/doi/10.1029/2009GL041203/abstract, 2010.

Karsten, U., Kirst, G. O., and Wiencke, C.: Dimethylsulphoniopropionate (DMSP) accumulation in green macroalgae from polar to temperate regions: interactive effects of light versus salinity and light versus temperature, Polar Biology, 12, 603–607, doi:10.1007/BF00236983, http://link.springer.com/article/10.1007/BF00236983, 1992.

Keller, M. D.: Dimethyl sulfide production and marine phytoplankton: the importance of species composition and cell size, Biological Oceanography, 6, 375–382, doi:10.1080/01965581.1988.10749540, http://www-tandfonline-com.ezproxy.library.uvic.ca/doi/abs/10.1080/01965581.1988.10749540, 1989.

Kiene, R. P. and Linn, L. J.: The fate of dissolved dimethylsulfoniopropionate (DMSP) in seawater: tracer studies using 35 S-DMSP, Geochimica et Cosmochimica Acta, 64, 2797–2810, http://www.sciencedirect.com/science/article/pii/S0016703700003999, 2000.

Kirst, G. O., Thiel, C., Wolff, H., Nothnagel, J., Wanzek, M., and Ulmke, R.: Dimethylsulfoniopropionate (DMSP) in icealgae and its possible biological role, Marine Chemistry, 35, 381–388, doi:10.1016/S0304-4203(09)90030-5, http://www.sciencedirect.com/science/article/pii/S0304420309900305, 1991.

Laroche, D., Vezina, A. F., Levasseur, M., Gosselin, M., Stefels, J., Keller, M. D., Matrai, P. A., and Kwint, R. L. J.: DMSP synthesis and exudation in phytoplankton: a modeling approach, Marine Ecology Progress Series, 180, 37–49, http://www.int-res.com/articles/meps/180/m180p037.pdf, 1999.

Leaitch, W. R., Sharma, S., Huang, L., Toom-Sauntry, D., Chivulescu, A., Macdonald, A. M., von Salzen, K., Pierce, J. R., Bertram, A. K., Schroder, J. C., Shantz, N. C., Chang, R. Y.-W., and Norman, A.-L.: Dimethyl sulfide control of the clean summertime Arctic aerosol and cloud, Elementa: Science of the Anthropocene, 1, 000 017, doi:10.12952/journal.elementa.000017, http://elementascience.org:80/article/info:doi/10.12952/journal.elementa.000017, 2013.

Leck, C. and Persson, C.: The central Arctic Ocean as a source of dimethyl sulfide Seasonal variability in relation to biological activity, Tellus B, 48, 156–177, doi:10.1034/j.1600-0889.1996.t01-1-00003.x, http://onlinelibrary.wiley.com.ezproxy.library.uvic.ca/doi/10.1034/j.1600-0889.1996.t01-1-00003.x/abstract, 1996.

Lefèvre, M., Vézina, A., Levasseur, M., and Dacey, J. W.: A model of dimethylsulfide dynamics for the subtropical North Atlantic, Deep Sea Research Part I: Oceanographic Research Papers, 49, 2221–2239, http://www.sciencedirect.com/science/article/pii/S0967063702001218, 2002.

Levasseur, M.: Impact of Arctic meltdown on the microbial cycling of sulphur, Nature Geoscience, 6, 691–700, doi:10.1038/ngeo1910, http://www.nature.com/doifinder/10.1038/ngeo1910, 2013.

Levasseur, M., Gosselin, M., and Michaud, S.: A new source of dimethylsulfide (DMS) for the Arctic atmosphere: Ice diatoms, Marine Biology, 121, 381–387, http://link.springer.com/article/10.1007/BF00346748, 1994.

Lindsay, R. W. and Rothrock, D. A.: Arctic sea ice leads from advanced very high resolution radiometer images, Journal of Geophysical Research: Oceans, 100, 4533–4544, doi:10.1029/94JC02393, http://onlinelibrary.wiley.com.ezproxy.library.uvic.ca/doi/10.1029/94JC02393/abstract, 1995.

Loose, B., Miller, L., Elliot, S., and Papakyriakou, T.: Sea ice biogeochemistry and material transport across the frozen interface, Oceanography, 24, 202–218, doi:10.5670/oceanog.2011.72, http://tos.org/oceanography/article/sea-ice-biogeochemistry-and-material-transport-across-the-frozen-interface, 2011.

Luce, M., Levasseur, M., Scarratt, M. G., Michaud, S., Royer, S.-J., Kiene, R., Lovejoy, C., Gosselin, M., Poulin, M., Gratton, Y., and Lizotte, M.: Distribution and microbial metabolism of dimethylsulfoniopropionate and dimethylsulfide during the 2007 Arctic ice minimum, Journal of Geophysical Research, 116, doi:10.1029/2010JC006914, http://doi.wiley.com/10.1029/2010JC006914, 2011.

Matrai, P. A. and Keller, M. D.: Total organic sulfur and dimethylsulfoniopropionate in marine phytoplankton: intracellular variations, Marine Biology, 119, 61–68, doi:10.1007/BF00350107, http://link.springer.com/article/10.1007/BF00350107, 1994.

Mortenson, E., Hayashida, H., Monahan, A. H., Steiner, N., Blais, M., Gale, M. A., Galindo, V., Gosselin, M., Hu, X., Lavoie, D., and Mundy, C. J.: A model-based analysis of physical and biological controls on ice algae and pelagic primary production in Resolute Passage, Elementa: Science of the Anthropocene, Submitted.

Motard-Côté, J., Levasseur, M., Scarratt, M. G., Michaud, S., Gratton, Y., Rivkin, R. B., Keats, K., Gosselin, M., Tremblay, J.-E., Kiene, R. P., and Lovejoy, C.: Distribution and metabolism of dimethylsulfoniopropionate (DMSP) and phylogenetic affiliation of DMSP-assimilating bacteria in northern Baffin Bay/Lancaster Sound, Journal of Geophysical Research: Oceans, 117, doi:10.1029/2011JC007330, http://doi.wiley.com/10.1029/2011JC007330, 2012.

Mundy, C., Gosselin, M., Gratton, Y., Brown, K., Galindo, V., Campbell, K., Levasseur, M., Barber, D., Papakyriakou, T., and Bélanger, S.: Role of environmental factors on phytoplankton bloom initiation under landfast sea ice in Resolute Passage, Canada, Marine Ecology Progress Series, 497, 39–49, doi:10.3354/meps10587, http://www.int-res.com/abstracts/meps/v497/p39-49/, 2014.

Mungall, E. L., Croft, B., Lizotte, M., Thomas, J. L., Murphy, J. G., Levasseur, M., Martin, R. V., Wentzell, J. J. B., Liggio, J., and Abbatt, J. P. D.: Dimethyl sulfide in the summertime Arctic atmosphere: measurements and source sensitivity simulations, Atmos. Chem. Phys., 16, 6665–6680, doi:10.5194/acp-16-6665-2016, http://www.atmos-chem-phys.net/16/6665/2016/, 2016.

Nightingale, P. D., Malin, G., Law, C. S., Watson, A. J., Liss, P. S., Liddicoat, M. I., Boutin, J., and Upstill-Goddard, R. C.: In situ evaluation of air-sea gas exchange parameterizations using novel conservative and volatile tracers, Global Biogeochemical Cycles, 14, 373–387, doi:10.1029/1999GB900091, http://onlinelibrary.wiley.com/doi/10.1029/1999GB900091/abstract, 2000.

Niki, T., Kunugi, M., and Otsuki, A.: DMSP-lyase activity in five marine phytoplankton species: its potential importance in DMS production, Marine Biology, 136, 759–764, doi:10.1007/s002279900235, http://link.springer.com.ezproxy.library.uvic.ca/article/10.1007/s002279900235, 2000.

Nomura, D., Koga, S., Kasamatsu, N., Shinagawa, H., Simizu, D., Wada, M., and Fukuchi, M.: Direct measurements of DMS flux from Antarctic fast sea ice to the atmosphere by a chamber technique, Journal of Geophysical Research: Oceans, 117, C04 011, doi:10.1029/2010JC006755, http://onlinelibrary.wiley.com/doi/10.1029/2010JC006755/abstract, 2012.

Pandis, S. N., Russell, L. M., and Seinfeld, J. H.: The relationship between DMS flux and CCN concentration in remote marine regions, Journal of Geophysical Research, 99, 16 945, doi:10.1029/94JD01119, http://doi.wiley.com/10.1029/94JD01119, 1994.

Quinn, P. K. and Bates, T. S.: The case against climate regulation via oceanic phytoplankton sulphur emissions, Nature, 480, 51–56, doi:10.1038/nature10580, http://www.nature.com/doifinder/10.1038/nature10580, 2011.

Rempillo, O., Seguin, A. M., Norman, A.-L., Scarratt, M., Michaud, S., Chang, R., Sjostedt, S., Abbatt, J., Else, B., Papakyriakou, T., Sharma, S., Grasby, S., and Levasseur, M.: Dimethyl sulfide air-sea fluxes and biogenic sulfur as a source of new aerosols in the Arctic fall, Journal of Geophysical Research: Atmospheres, 116, D00S04, doi:10.1029/2011JD016336, http://onlinelibrary.wiley.com.ezproxy.library.uvic.ca/doi/10.1029/2011JD016336/abstract, 2011.

Russell, L. M., Pandis, S. N., and Seinfeld, J. H.: Aerosol production and growth in the marine boundary layer, Journal of Geophysical Research, 99, 20 989–21 003, http://authors.library.caltech.edu/51128/, 1994.

Saltzman, E. S., King, D. B., Holmen, K., and Leck, C.: Experimental determination of the diffusion coefficient of dimethylsulfide in water, Journal of Geophysical Research: Oceans, 98, 16 481–16 486, doi:10.1029/93JC01858, http://onlinelibrary.wiley.com.ezproxy.library.uvic.ca/doi/10.1029/93JC01858/abstract, 1993.

Sharma, S., Barrie, L. A., Plummer, D., McConnell, J. C., Brickell, P. C., Levasseur, M., Gosselin, M., and Bates, T. S.: Flux estimation of oceanic dimethyl sulfide around North America, Journal of Geophysical Research: Atmospheres, 104, 21 327–21 342, doi:10.1029/1999JD900207, http://onlinelibrary.wiley.com/doi/10.1029/1999JD900207/abstract, 1999.

Sharma, S., Chan, E., Ishizawa, M., Toom-Sauntry, D., Gong, S. L., Li, S. M., Tarasick, D. W., Leaitch, W. R., Norman, A., Quinn, P. K., Bates, T. S., Levasseur, M., Barrie, L. A., and Maenhaut, W.: Influence of transport and ocean ice extent on biogenic aerosol sulfur in the Arctic atmosphere: MSA IN THE ARCTIC, Journal of Geophysical Research: Atmospheres, 117, n/a–n/a, doi:10.1029/2011JD017074, http://doi.wiley.com/10.1029/2011JD017074, 2012.

Shaw, G. E.: Bio-controlled thermostasis involving the sulfur cycle, Climatic Change, 5, 297–303, http://link.springer.com/article/10.1007/BF02423524, 1983.

Simo, R.: Production of atmospheric sulfur by oceanic plankton: biogeochemical, ecological and evolutionary links, Trends in Ecology & Evolution, 16, 287–294, http://www.sciencedirect.com/science/article/pii/S0169534701021528, 2001.

Simo, R. and Pedros-Alio, C.: Short-term variability in the open ocean cycle of dimethylsulfide, Global Biogeochemical Cycles, 13, 1173–1181, doi:10.1029/1999GB900081, http://onlinelibrary.wiley.com/doi/10.1029/1999GB900081/abstract, 1999.

Stefels, J.: Physiological aspects of the production and conversion of DMSP in marine algae and higher plants, Journal of Sea Research, 43, 183–197, doi:10.1016/S1385-1101(00)00030-7, http://www.sciencedirect.com/science/article/pii/S1385110100000307, 2000.

Stefels, J. and van Leeuwe, M. A.: Effects of Iron and Light Stress on the Biochemical Composition of Antarctic Phaeocystis Sp. (prymnesiophyceae). I. Intracellular Dmsp Concentrations, Journal of Phycology, 34, 486–495, doi:10.1046/j.1529-8817.1998.340486.x, http://onlinelibrary.wiley.com.ezproxy.library.uvic.ca/doi/10.1046/j.1529-8817.1998.340486.x/abstract, 1998.

Stefels, J., Steinke, M., Turner, S., Malin, G., and Belviso, S.: Environmental constraints on the production and removal of the climatically active gas dimethylsulphide (DMS) and implications for ecosystem modelling, Biogeochemistry, 83, 245–275, doi:10.1007/s10533-007-9091-5, http://link.springer.com.ezproxy.library.uvic.ca/article/10.1007/s10533-007-9091-5, 2007.

Stefels, J., Carnat, G., Dacey, J. W. H., Goossens, T., Elzenga, J. T. M., and Tison, J.-L.: The analysis of dimethylsulfide and dimethylsulfoniopropionate in sea ice: Dry-crushing and melting using stable isotope additions, Marine Chemistry, 128–129, 34–43, doi:10.1016/j.marchem.2011.09.007, http://www.sciencedirect.com/science/article/pii/S0304420311001046, 2012.

Steiner, N. and Denman, K.: Parameter sensitivities in a 1-D model for DMS and sulphur cycling in the upper ocean, Deep Sea Research Part I: Oceanographic Research Papers, 55, 847–865, doi:10.1016/j.dsr.2008.02.010, http://linkinghub.elsevier.com/retrieve/pii/S0967063708000617, 2008.

Steiner, N., Denman, K., McFarlane, N., and Solheim, L.: Simulating the coupling between atmosphere–ocean processes and the planktonic ecosystem during SERIES, Deep Sea Research Part II: Topical Studies in Oceanography, 53, 2434–2454, doi:10.1016/j.dsr2.2006.05.030, http://linkinghub.elsevier.com/retrieve/pii/S0967064506002037, 2006.

Steiner, N. S., Lee, W. G., and Christian, J. R.: Enhanced gas fluxes in small sea ice leads and cracks: Effects on CO 2 exchange and ocean acidification, Journal of Geophysical Research: Oceans, 118, 1195–1205, doi:10.1002/jgrc.20100, http://onlinelibrary.wiley.com.ezproxy.library.uvic.ca/doi/10.1002/jgrc.20100/abstract, 2013.

Sunda, W., Kieber, D. J., Kiene, R. P., and Huntsman, S.: An antioxidant function for DMSP and DMS in marine algae, Nature, 418, 317–320, doi:10.1038/nature00851, http://www.nature.com.ezproxy.library.uvic.ca/nature/journal/v418/n6895/abs/nature00851.html, 2002.

Sunda, W. G., Hardison, R., Kiene, R. P., Bucciarelli, E., and Harada, H.: The effect of nitrogen limitation on cellular DMSP and DMS release in marine phytoplankton: climate feedback implications, Aquatic Sciences, 69, 341–351, doi:10.1007/s00027-007-0887-0, http://link.springer.com/10.1007/s00027-007-0887-0, 2007.

Taalba, A., Xie, H., Scarratt, M. G., Bélanger, S., and Levasseur, M.: Photo-oxidation of Dimethylsulfide (DMS) in the Western Canadian Arctic, AGU Fall Meeting Abstracts, 10, 6793– 6806, http://adsabs.harvard.edu/abs/2012AGUFMOS31B1724T, 2012.

Toole, D. A., Kieber, D. J., Kiene, R. P., White, E. M., Bisgrove, J., del Valle, D. A., and Slezak, D.: High dimethylsulfide photolysis rates in nitrate-rich Antarctic waters, Geophysical Research Letters, 31, L11 307, doi:10.1029/2004GL019863, http://onlinelibrary.wiley.com/doi/10.1029/2004GL019863/abstract, 2004.

Uzuka, N.: A time series observation of DMSP production in the fast ice zone near Barrow, http://ir.library.tohoku.ac.jp/re/handle/10097/45420, 2003.

van Rijssel, M. and Gieskes, W. W. C.: Temperature, light, and the dimethylsulfoniopropionate (DMSP) content of Emiliania huxleyi (Prymnesiophyceae), Journal of Sea Research, 48, 17–27, doi:10.1016/S1385-1101(02)00134-X, http://www.sciencedirect.com/science/article/pii/S138511010200134X, 2002.

Vancoppenolle, M., Goosse, H., de Montety, A., Fichefet, T., Tremblay, B., and Tison, J.-L.: Modeling brine and nutrient dynamics in Antarctic sea ice: The case of dissolved silica, Journal of Geophysical Research, 115, doi:10.1029/2009JC005369, http://doi.wiley.com/10.1029/2009JC005369, 2010.

Zemmelink, H. J., Dacey, J. W. H., Houghton, L., Hintsa, E. J., and Liss, P. S.: Dimethylsulfide emissions over the multi-year ice of the western Weddell Sea, Geophysical Research Letters, 35, L06 603, doi:10.1029/2007GL031847, http://onlinelibrary.wiley.com.ezproxy.library.uvic.ca/doi/10.1029/2007GL031847/abstract, 2008.

Biogeosciences Discuss., doi:10.5194/bg-2016-399, 2016
Manuscript under review for journal Biogeosciences
Published: 4 October 2016

Biogeosciences Discussions Open Access EGU

Table 1. List of the coupled sea ice-ocean sulfur cycle model variables and parameters

Symbol	Description	Units	Value
Variable			
$DMSPp$, $DMSPp_{wc}$	DMSPp concentration	nmol L^{-1}	
$DMSPd$, $DMSPd_{wc}$	DMSPd concentration	nmol L^{-1}	
DMS, DMS_{wc}	DMS concentration	nmol L^{-1}	
Γ_{z1}^{p1}	Grazing rate of zooplankton on phytoplankton	d^{-1}	
L_{nut}, L_{nut}^{p1}, L_{nut}^{p2}	Nutrient limitation index	-	
PAR, PAR_{wc}	Photosynthetically active radiation	W m^{-2}	
$R_{flushing}$	Flushing rate	m s^{-1}	
μ, μ_{p1}, μ_{p2}	Algal growth rate	s^{-1}	
T_{z_0}	Seawater temperature in the uppermost layer	$^\circ$ C	
U_{10}	Wind speed at 10 m	m s^{-1}	
Parameter			
f_{active}, f_{active}^{p1}, f_{active}^{p2}	Active exudation fraction	-	0.05, 0.05, 0.05
f_{sloppy}^{z1}, f_{sloppy}^{z2}	Sloppy feeding fraction	-	0.3, 0.3
f_{yield}, f_{yield}^{wc}	Bacterial yield	-	0.2, 0.2
h_{bi}	Thickness of the bottom ice	m	0.03
$h_{photolysis}$, $h_{photolysis}^{wc}$	Photolysis half-saturation constant	W m^{-2}	1, 1
h_{z_0}	Thickness of the uppermost layer of the water column	m	1
k_{dms}, k_{dms}^{wc}	Bacterial DMS consumption rate constant	d^{-1}	0.2, 0.5
k_{dmspd}, k_{dmspd}^{wc}	Bacterial DMSPd consumption rate constant	d^{-1}	1, 5
k_{free}, k_{free}^{wc}	free DMSP-lyase rate constant	d^{-1}	0.02, 0.02
k_{lysis}, k_{lysis}^{p1}, k_{lysis}^{p2}	Cell lysis rate constant	d^{-1}	0.03, 0.03, 0.03
$k_{photolysis}$, $k_{photolysis}^{wc}$	Photolysis rate constant	d^{-1}	0.1, 0.1
q, q_{p1}, q_{p2}	Intracellular DMSP-to-Chl a ratio	nmol S:μg Chl a	9.5, 100, 9.5

Table 2. Sensitivity of simulated under-ice DMS to the incorporation of the sea-ice sulfur cycle and ecosystem. Overall changes were calculated by taking the difference in the time-integrated under-ice DMS concentrations between the two runs of interest and dividing it by the time-integrated under-ice DMS concentration in the run being subtracted.

Runs to be compared (Implications of the comparioson)	Maximum concentration difference [nmol L^{-1}]	Overall change [%]
Standard - NoIceSul (Impact of sea-ice sulfur cycle)	2.1	21
NoIceSul - NoIceBgc (Impact of sea-ice ecosystem)	4.3	-16
Standard - NoIceBgc (Impact of sea-ice biogeochemistry)	5.7	2

Biogeosciences Discuss., doi:10.5194/bg-2016-399, 2016
Manuscript under review for journal Biogeosciences
Published: 4 October 2016

Table 3. Sensitivity of simulated bottom-ice and under-ice DMS to doubling the model parameter of the sea-ice sulfur cycle. Changes in the bottom-ice and under-ice DMS were calculated by subtracting the time-integrated DMS in the sensitivity run from the time-integrated DMS in the standard run and dividing the difference by the time-integrated DMS in the standard run.

Run	Description	Change in the bottom-ice DMS	Change in the under-ice DMS
Case 1	Doubling the intracellular DMSP:Chl a ratio	100 %	18 %
Case 2	Doubling the DMS yield fraction	91 %	13 %
Case 3	Doubling the bacterial DMSPd consumption rate constant	-2 %	-2 %
Case 4	Doubling the bacterial DMS consumption rate constant	-44 %	-6 %
Case 5	Doubling the photolysis rate constant	-8 %	-3 %

Table 4. Sensitivity of simulated sea-air DMS fluxes to the open-water fraction and to the incorporation of sea-ice biogeochemistry. Overall changes were calculated by taking the difference between the two runs of interest and dividing it by the cumulative flux in the subtracted run.

Open-water fraction [-]	0.02 (Small lead)	0.1 (Large lead)	0.5 (Near ice margin)	1 (At ice margin)
	Maximum flux [μmol m^{-2} d^{-1}]			
(Standard)	0.3	1.2	4.9	8.1
	Maximum flux difference [μmol m^{-2} d^{-1}]			
(Standard - NoIceSul)	0.1	0.3	1.2	1.9
(NoIceSul - NoIceBgc)	0.1	0.5	2.3	4.0
(Standard - NoIceBgc)	0.2	0.8	3.4	5.6
	Overall change [%]			
(Standard - NoIceSul)	24	28	29	30
(NoIceSul - NoIceBgc)	-13	-11	-9	-7
(Standard - NoIceBgc)	8	13	17	20

Biogeosciences Discuss., doi:10.5194/bg-2016-399, 2016
Manuscript under review for journal Biogeosciences
Published: 4 October 2016

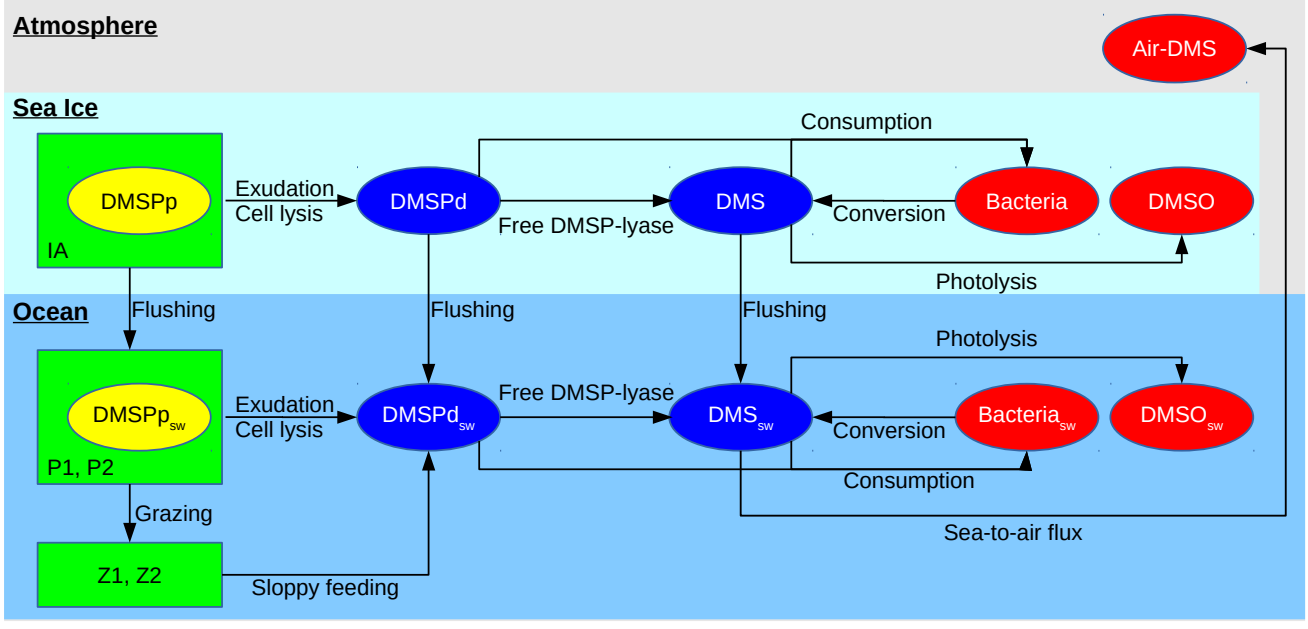

Figure 1. Schematic of the sea-ice and oceanic components of the sulfur cycle module. Variables in blue (yellow) are simulated prognostically (diagnostically), while the variables in red are not simulated but the relevant processes are parameterized. Variables in green are simulated prognostically by the ecosystem model. Arrows represent the physical and biogeochemical fluxes parameterized in the module.

Biogeosciences Discuss., doi:10.5194/bg-2016-399, 2016
Manuscript under review for journal Biogeosciences
Published: 4 October 2016

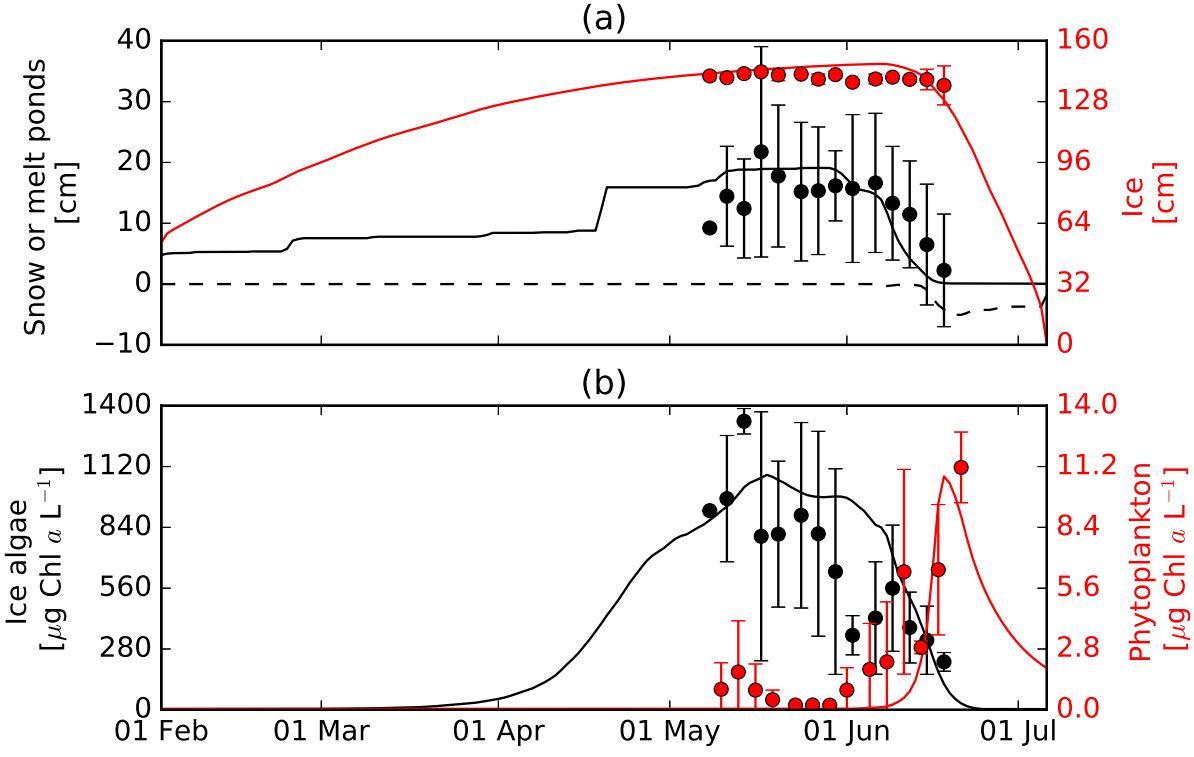

Figure 2. Simulated (lines) and observed (dots and bars) time series of (a) snow (black solid) and melt pond (black dashed) depths [cm] and ice thickness [cm] (red), and (b) ice algal biomass [μg Chl a l^{-1}] in the bottom 3 cm ice (black) and phytoplankton biomass [μg Chl a l^{-1}] averaged over the upper 10 m water column (red) in Resolute Passage during 2010. In (a), the negative values present the depth of melt ponds. Also in (a), the observed values show the average (dots) and 1 standard deviation (vertical bars) of samples collected at three sites of high (>20 cm), medium (10-20 cm), and low (<10 cm) snow cover. In (b), the observed ice algal biomass shows the average (black dots) and 1 standard deviation (vertical bars) of samples collected in ice cores under high, medium, and low snow cover sites, while the observed phytoplankton biomass shows the average (red dots) with $\pm$ 1 standard deviation (vertical bars) of samples collected in seawater at 1.5, 2, 5, and 10 m depth.

Biogeosciences Discuss., doi:10.5194/bg-2016-399, 2016
Manuscript under review for journal Biogeosciences
Published: 4 October 2016

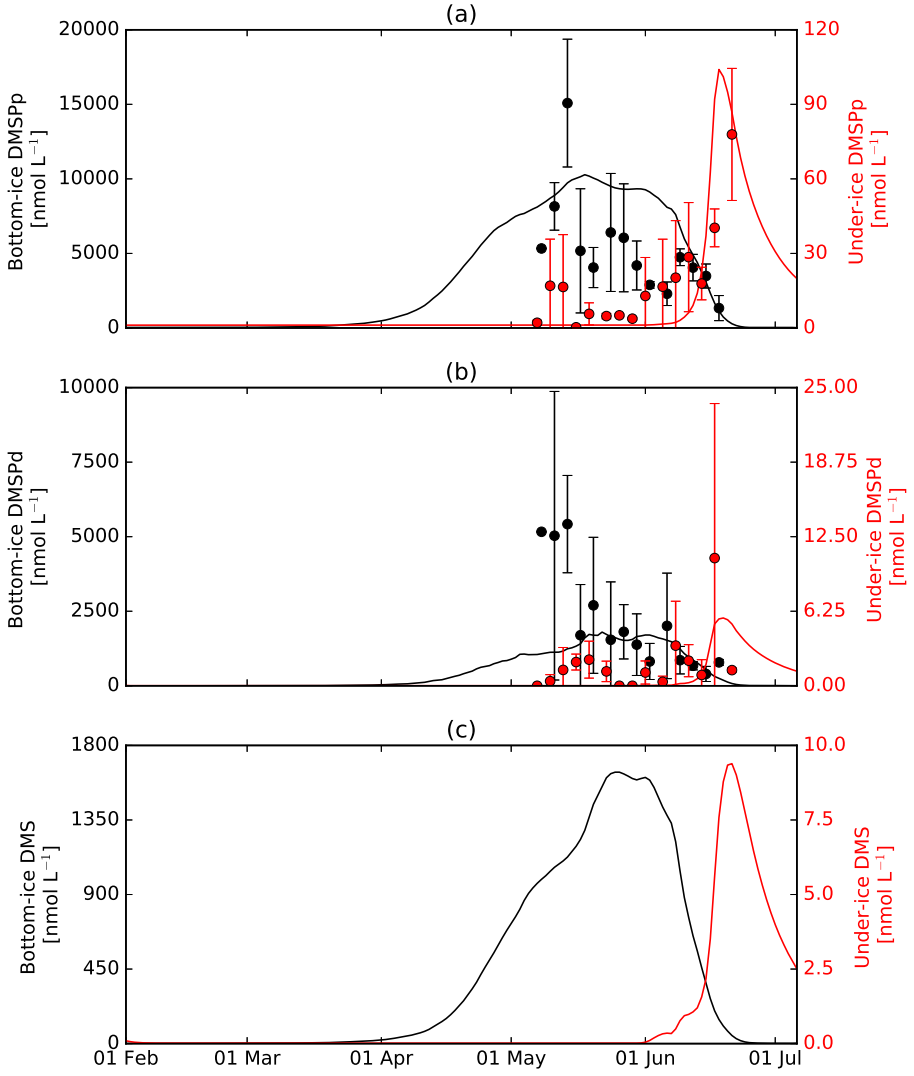

Figure 3. Simulated (lines) and observed (dots and bars) time series of (a) DMSPp, (b) DMSPd, and (c) DMS concentrations [nmol L^{-1}] in the bottom 3 cm ice (black) and averaged over the upper 10 m water column (red) in Resolute Passage during 2010. The observed bottom-ice values show the average (black dots) and 1 standard deviation (vertical bars) of samples collected in ice cores under high, medium, and low snow cover sites. The observed upper 10 m water column values show the average (red dots) with ± 1 standard deviation (vertical bars) of samples collected in seawater at 1.5, 2, 5, and 10 m depth.

Biogeosciences Discuss., doi:10.5194/bg-2016-399, 2016
Manuscript under review for journal Biogeosciences
Published: 4 October 2016

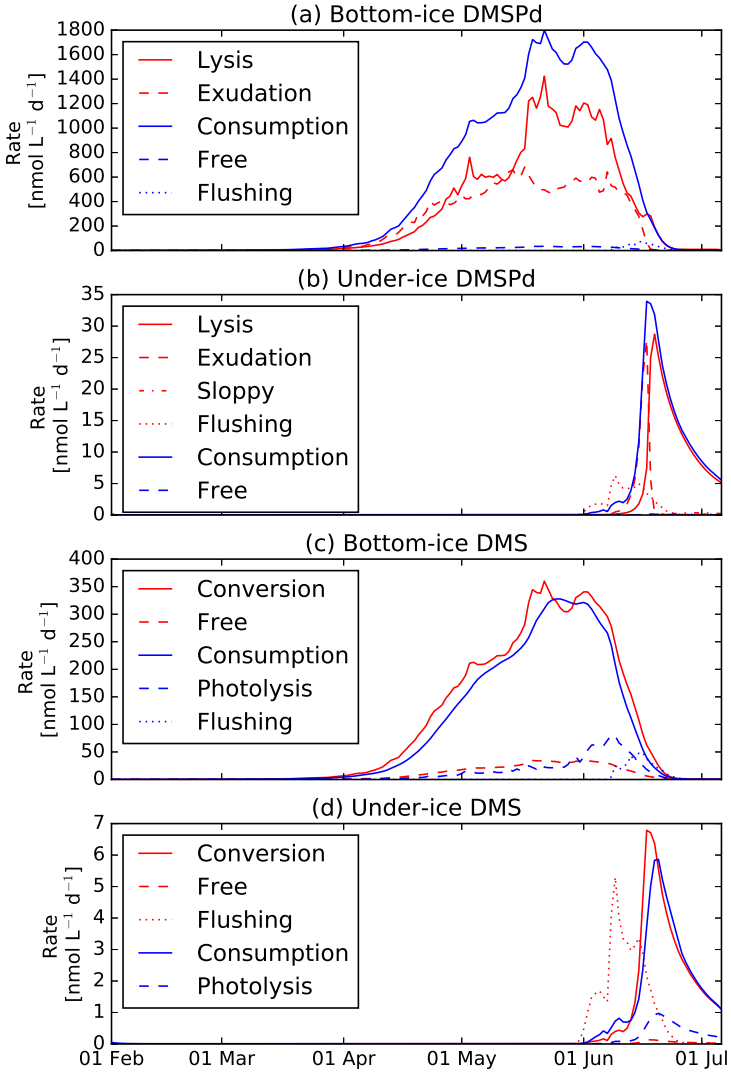

Figure 4. Simulated time series of daily mean production (red) and removal (blue) rates [nmol L^{-1} d^{-1}] of (a and b) DMSPd and (c and d) DMS (a and c) in the bottom 3 cm ice and (b and d) in the uppermost layer (0.5 m below the ice) of the water column. In (a) and (b), the sources for DMSPd are cell lysis (Lysis; solid red), exudation (Exudation; dashed red), and sloppy feeding (Sloppy; dash-dot red in (b) only) while its sinks are bacterial DMSPd consumption (Consumption; solid blue) and free DMSP-lyase (Free; dashed blue). In (c) and (d), the sources for DMS are bacterial DMSPd-to-DMS conversion (Conversion; solid red) and free DMSP-lyase (Free; dashed red), while its sinks are bacterial DMS consumption (Consumption; solid blue) and photolysis (Photolysis; dashed blue). Flushing (dotted) is a sink for the bottom-ice DMSPd (a) and DMS (c), while it is a source for the under-ice DMSPd (b) and DMS (d).

Biogeosciences Discuss., doi:10.5194/bg-2016-399, 2016
Manuscript under review for journal Biogeosciences
Published: 4 October 2016

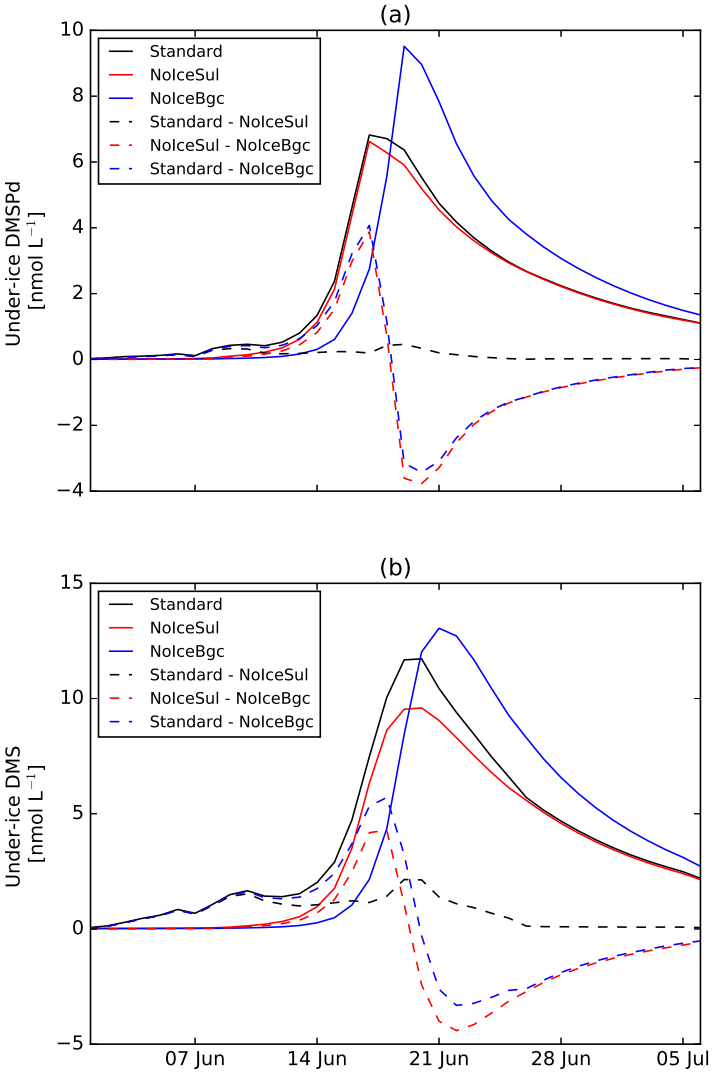

Figure 5. Simulated time series of (a) DMSPd and (b) DMS concentrations [nmol L^{-1}] in the uppermost layer (0.5 m below the ice) of the water column during the melt period in 2010 for the standard run (Standard) and the sensitivity runs that exluded the sea-ice sulfur cycle (NoIceSul) and both the sea-ice sulfur cycle and ecosystem (NoIceBgc). Dashed lines represent the concentration difference between the two runs of interest. Positive differences represent enhancement in the concentration due to the incorporation of sea-ice sulfur cycle (Standard - NoIceSul), sea-ice ecosystem (NoIceBgc - NoIceSul), and both sea-ice sulfur cycle and ecosystem (Standard - NoIceBgc), respectively, while negative values represent reduction.

Biogeosciences Discuss., doi:10.5194/bg-2016-399, 2016
Manuscript under review for journal Biogeosciences
Published: 4 October 2016

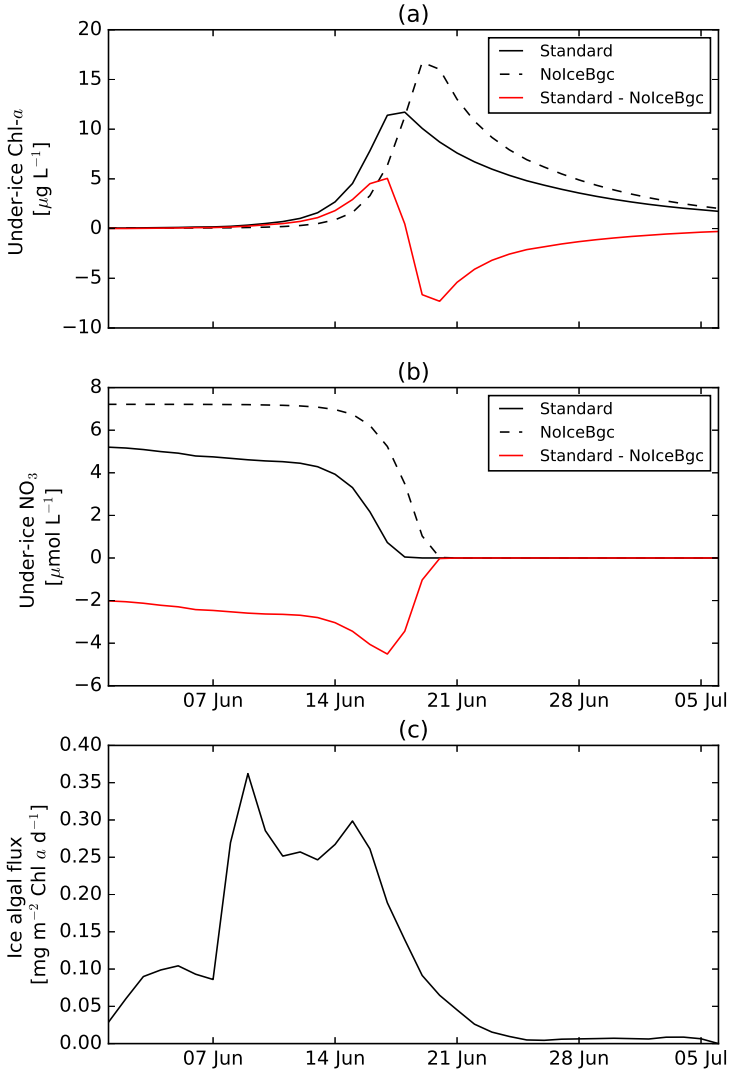

Figure 6. Simulated time series of (a) phytoplankton biomass [μg Chl a L^{-1}] and (b) nitrate concentration [μmol L^{-1}] in the uppermost layer (0.5 m below the ice) of the water column during the melt period in 2010 for the standard run (Standard) and the sensitivity run that exluded both the sea-ice sulfur cycle and ecosystem (NoIceBgc). (c) Ice algal flux [mg Chl a m^{-2} d^{-1}] entering the large phytoplankton pool in the uppermost layer of the water column. In (a) and (b), red lines represent the respective differences in phytoplankton biomass and nitrate concentration between the standard and sensitivity runs.

Biogeosciences Discuss., doi:10.5194/bg-2016-399, 2016
Manuscript under review for journal Biogeosciences
Published: 4 October 2016

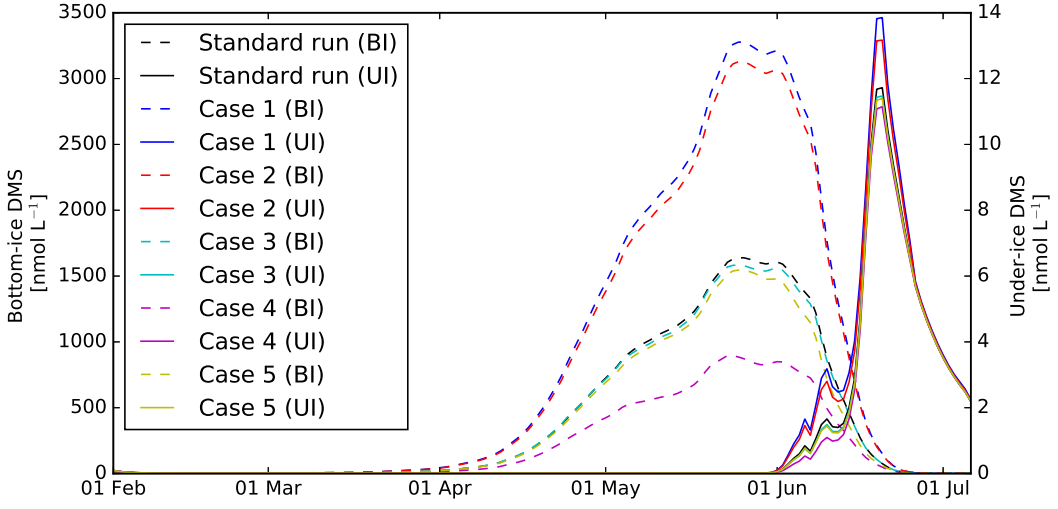

Figure 7. Simulated time series of bottom-ice (BI) and under-ice (UI; 0.5 m below the ice) DMS concentrations [nmol L^{-1}] during 2010 for: the standard run; Case 1: doubling the intracellular DMSP:Chl a ratio; Case 2: doubling the DMS yield fraction; Case 3: doubling the bacterial DMSPd consumption rate constant; Case 4: doubling the bacterial DMS consumption rate constant; and Case 5: doubling the photolysis rate constant.

Biogeosciences Discuss., doi:10.5194/bg-2016-399, 2016
Manuscript under review for journal Biogeosciences
Published: 4 October 2016

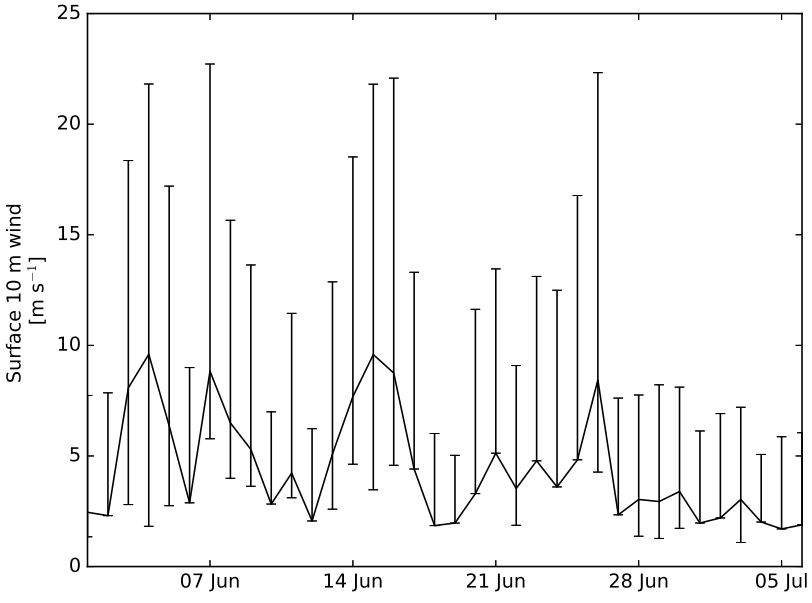

Figure 8. Time series of daily mean surface 10 wind speed [m s^{-1}] observed at the Resolute airport during the melt period in 2010. The upper and lower vertical bars associated with the daily mean values represent the daily maximum and minimum values, respectively.

Biogeosciences Discuss., doi:10.5194/bg-2016-399, 2016
Manuscript under review for journal Biogeosciences
Published: 4 October 2016

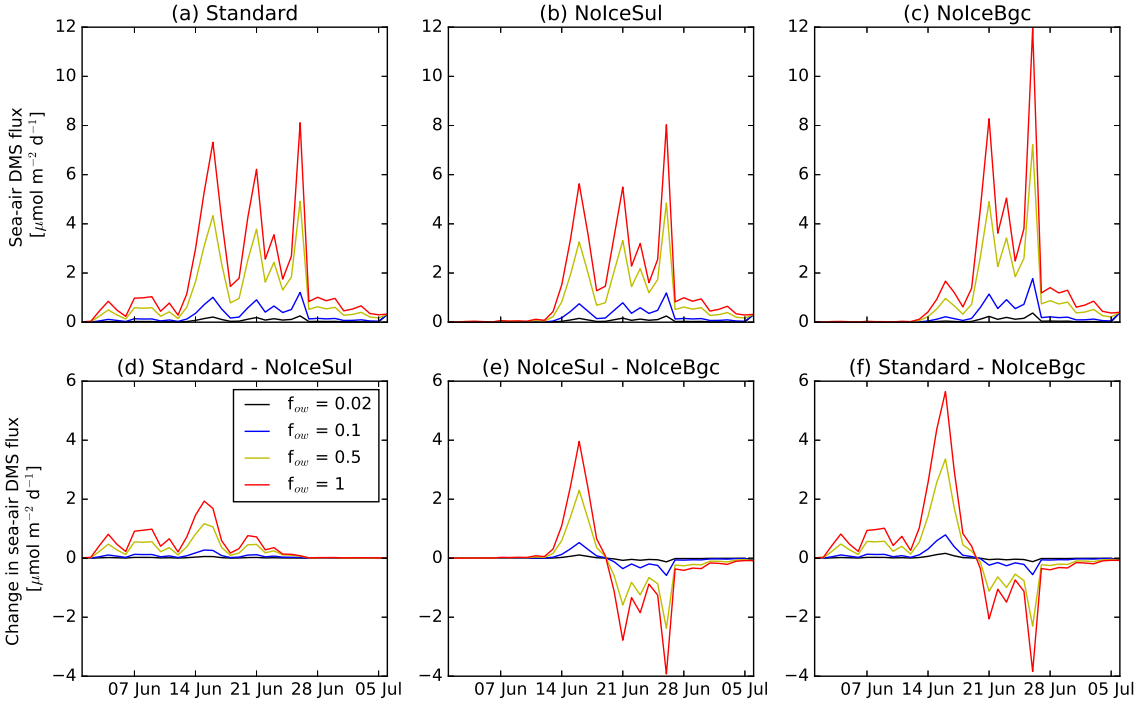

Figure 9. Simulated time series of sea-air DMS fluxes [μmol m^{-2} d^{-1}] for (a) the standard run and the sensitivity runs that excluded (b) the sea-ice sulfur cycle (NoIceSul) and (c) both the sea-ice sulfur cycle and ecosystem (NoIceBgc) and the flux difference between (d) the standard and NoIceSul runs, (e) the NoIceSul and NoIceBgc runs, and (f) the standard and NoIceBgc runs during the melt period in 2010. In (d), (e), and (f), positive values represent enhancement in the simulated flux due to the incorporation of sea-ice sulfur cycle, ecosystem, and both sulfur cycle and ecosystem, respectively, while negative values represent reduction.